AGU PUBLICATIONS

Geochemistry, Geophysics, Geosystems

RESEARCH ARTICLE
10.1002/2015GC006209

Key Points:
- The magnetostratigraphically sampled section in the Aktoprak basin is most likely Chattian in age
- Isotopic data suggest a subtropical, open freshwater paleoenvironment and no orographic barrier
- Partial, post-tilting remagnetization was controlled by clay content (i.e., permeability related)

Supporting Information:
- Supporting Information S1
- Data Set S1
- Data Set S2
- Data Set S3

Correspondence to:
M. J. M. Meijers,
meijersmaud@gmail.com

Citation:
Meijers, M. J. M., B. E. Strauss, M. Özkaptan, J. M. Feinberg, A. Mulch, D. L. Whitney, and N. Kaymakçı (2016), Age and paleoenvironmental reconstruction of partially remagnetized lacustrine sedimentary rocks (Oligocene Aktoprak basin, central Anatolia, Turkey), *Geochem. Geophys. Geosyst.*, *17*, 914–939, doi:10.1002/2015GC006209.

Received 2 DEC 2015
Accepted 5 FEB 2016
Accepted article online 12 FEB 2016
Published online 15 MAR 2016

© 2016. American Geophysical Union. All Rights Reserved.

Age and paleoenvironmental reconstruction of partially remagnetized lacustrine sedimentary rocks (Oligocene Aktoprak basin, central Anatolia, Turkey)

Maud J. M. Meijers[1,2,3], Becky E. Strauss[2], Murat Özkaptan[5], Joshua M. Feinberg[2], Andreas Mulch[4,6], Donna L. Whitney[1], and Nuretdin Kaymakçı[5]

[1]Department of Earth Sciences, University of Minnesota, Minneapolis, Minnesota, USA, [2]Department of Earth Sciences, Institute for Rock Magnetism, University of Minnesota, Minneapolis, Minnesota, USA, [3]Now at Senckenberg Biodiversity and Climate Research Centre (BiK-F), Frankfurt, Germany, [4]Senckenberg Biodiversity and Climate Research Centre (BiK-F), Frankfurt, Germany, [5]Department of Geological Engineering, Faculty of Engineering, Middle East Technical University, Ankara, Turkey, [6]Institute of Geosciences, Goethe University Frankfurt, Frankfurt, Germany

Abstract The age and paleoenvironmental record of lacustrine deposits in the Aktoprak basin of south-central Turkey provides information about the evolution of topography, including the timing of development of an orographic rain shadow caused by uplift of the mountain ranges fringing the Central Anatolian Plateau. New magnetostratigraphy-based age estimates, in combination with existing biostratigraphic ages, suggest that the partially remagnetized Kurtulmuş Tepe section of the basin is Chattian (Upper Oligocene). The mean carbon and oxygen stable isotope ratios ($\delta^{18}O = 24.6 \pm 2.0$ ‰, $\delta^{13}C = -4.9 \pm 1.1$‰) are largely constant through the section and indicative of a subtropical, open freshwater lake. These isotopic values are also similar to those of the Chattian Mut basin to the south, on the Mediterranean side of the modern orographic barrier (Tauride Mountains), and indicate absence of an orographic barrier during Late Oligocene basin deposition. Post-depositional partial remagnetization occurred after tilting of the basin sequence and was mineralogically controlled, affecting grey, carbonate-rich rocks (average $\%CaCO_3 = 82$), whereas interlayered pink carbonate-poor rocks (average $\%CaCO_3 = 38$) carry a primary, pretilt magnetization. The pink rocks are rich in clay minerals that may have reduced the permeability of these rocks that carry a primary magnetization, concentrating basinal fluid flow in the carbonate-rich grey layers and leading to the removal and reprecipitation of magnetic minerals. The normal and reverse polarities recorded by the remagnetized rocks suggest that remagnetization occurred over a protracted period of time.

1. Introduction

Beginning in the Oligocene, vast parts of Central Anatolia were covered with lake systems [e.g., *Lüttig and Steffens*, 1975; *Krijgsman et al*., 1996; *Jaffey and Robertson*, 2005], relics of which can presently be found in the rock record (Figure 1a). At present, however, only a small fraction of the surface area of Central Anatolia is covered with lakes, the largest of which is the highly evaporative Tuz Gölü (Salt Lake, Figure 1a). Lacustrine deposits provide a rich paleoenvironmental record of climate, and furnish information about tectonic processes that have a profound effect on climate through topographic changes, such as the uplift and evolution of orogenic plateaux and orographic barriers to precipitation.

The geographical extent of the paleolake system in Anatolia was affected throughout the Cenozoic by the interplay of paleoenvironmental (climatic) and tectonic processes in this geologically active region. Regional climatic changes in the Eastern Mediterranean accompanied global changes such as the onset of glaciations in the Late Eocene, as well as relatively warm periods in the Late Oligocene and mid-Miocene [e.g., *Zachos et al*., 2001; *Gierlowski-Kordesch*, 2010]. The tectonic evolution of the Eastern Mediterranean region has been dominated by ongoing Africa-Eurasia convergence since the Jurassic. Driven by subduction and crustal shortening owing to continental collision, this convergence ultimately facilitated the development of the Central Anatolian Plateau (CAP; today at ~1000 m elevation). The CAP is bordered to its north and south by mountain ranges (the Pontide and Tauride Mountains, respectively)

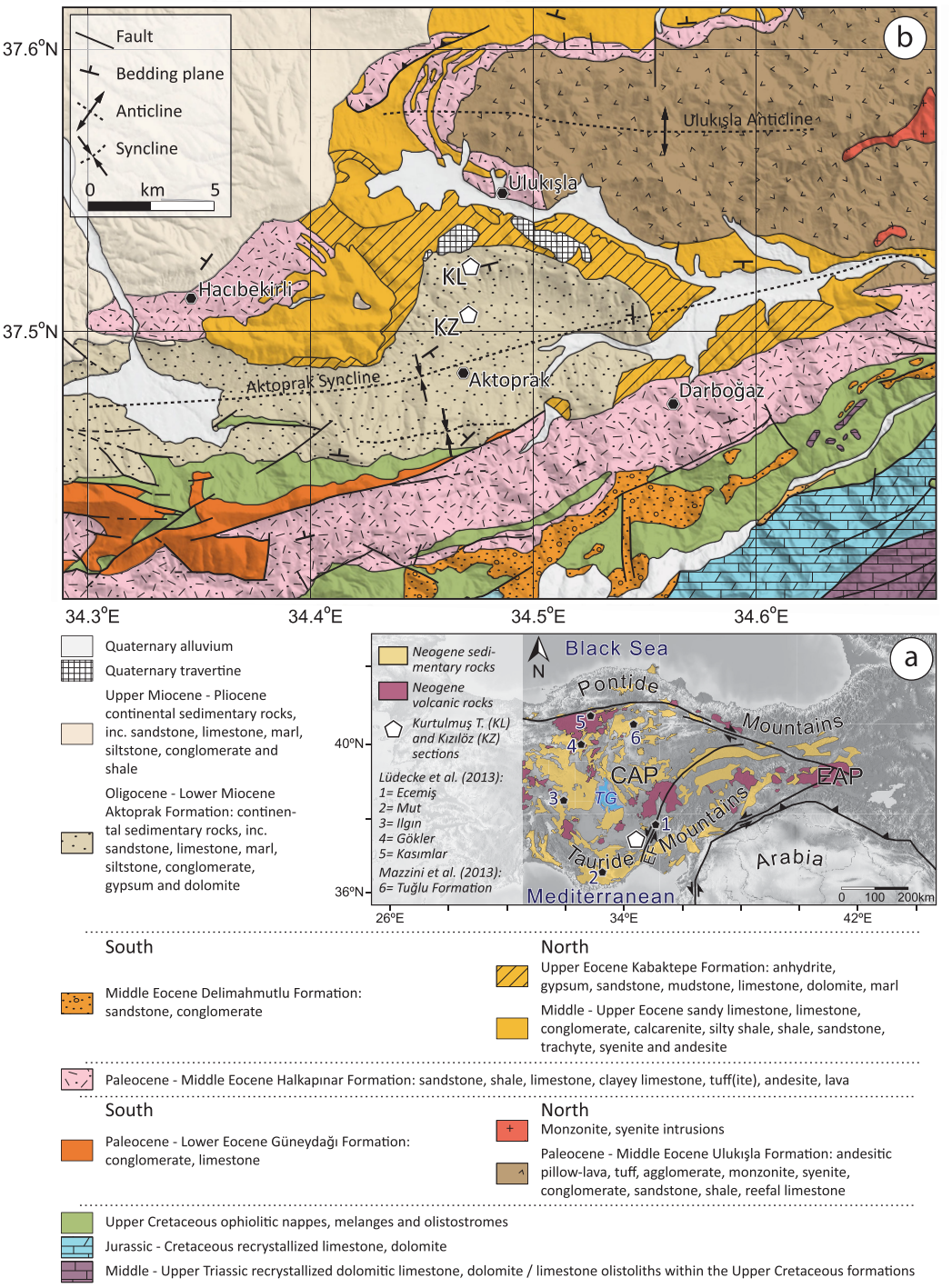

Figure 1. (a) Location of the Aktoprak basin (white pentagon) within south-central Turkey in the eastern Mediterranean region. The Aktoprak basin is situated on the Central Anatolian Plateau (CAP), north of the Tauride Mountains and south of the Central Anatolian Crystalline Complex (CACC). Polygons indicate the widespread Neogene sedimentary rocks (in yellow) and Neogene volcanic rocks (in purple). EF= Ecemiş Fault, TG= Tuz Gölü. Numbered sites indicate the location of the sampled sections of *Lüdecke et al.* [2013]. (b) Geological map of the Aktoprak basin and its surroundings projected onto a Digital Elevation Model (DEM). Pentagons indicate the location of the Kurtulmuş Tepe (KL) and Kızılöz (KZ) sections with the basin. The basin forms a broad syncline south of the town of Ulukışla. Geological map after *Atabey et al.* [1990], *Ulu* [2009], and *Alan et al.* [2011a, 2012b].

that locally reach up to 3000 m elevation. The development of the plateau and the Pontide and Tauride margins after ~8 Ma [e.g., *Yıldırım et al.*, 2011; *Schildgen et al.*, 2012a,b] led to the current semiarid conditions in the plateau interior (300–500 mm annual precipitation) [*Schemmel et al.*, 2013].

Carbon ($\delta^{13}C$) and oxygen ($\delta^{18}O$) isotope measurements on authigenic minerals that formed in paleolakes can be collected to investigate climatic (temperature, precipitation) and tectonic (changes in drainage basin, development of rain shadow) effects on lake water composition and lake hydrology. $\delta^{13}C$ and $\delta^{18}O$ data may elucidate environmental change such as transitions from open to closed lake systems, the emergence of orographic barriers, and onset of evaporitic conditions.

The limited number of continental basins in central Anatolia for which absolute ages have been obtained [e.g., *Le Pennec et al*., 2005; *Krijgsman et al*., 1996; *Koç et al*., 2012; *Gülyüz et al*., 2013; *Lüdecke et al*., 2013; *Mazzini et al*., 2013] makes spatio-temporal environmental and tectonostratigraphic reconstructions across Anatolia challenging. To determine the paleoenvironmental conditions and paleotopography from the isotopic composition of lacustrine deposits, it is important to obtain ages for the sedimentary deposits. Biostratigraphy provides sparse age information (e.g., from ostracoda and gastropods), although in the paleolake deposits of Central Anatolia, this approach typically provides only broad age constraints (e.g., Late Oligocene to Early Miocene for the Aktoprak Basin) [*Blumenthal*, 1956]. Biostratigraphic age constraints based on mammalian fossils are widely available in Turkey from the New and Old Worlds Database of Fossil Mammals (NOW) [*Fortelius*, 2013], but nonexistent for the Aktoprak basin. In the absence of volcanic ash or other dateable materials in lacustrine sequences, magnetostratigraphy is the only available dating technique. In this study, we use an integrative approach to reconstruct the paleoenvironmental history and determine the chronology of the lacustrine sedimentary rocks of the central Anatolian Aktoprak basin (Figure 1).

The nonmarine sedimentary rocks of the Aktoprak basin are exposed in a syncline with a roughly east-west oriented and west plunging fold axis located south of Ulukışla (Figure 1b). The basin formed unconformably atop volcano-sedimentary units of Paleocene-Eocene age [*Clark and Robertson*, 2005; *Jaffey and Robertson*, 2005]. The ages assigned to the sedimentary rocks exposed within the Aktoprak basin are based on nonmarine fossil records, and therefore are not well constrained. The age of the Kurtulmuş Tepe Formation is based on gastropods and ostracoda and is estimated to be Chattian (Late Oligocene) or Aquitanian (earliest Miocene). After a compressional tectonic phase that produced tilting and folding of the Aktoprak basin sedimentary rocks, Upper Miocene to Pliocene lacustrine sediments were deposited. These youngest sediments are currently gently dipping to the northwest [*Riveline et al*., 1990; *Jaffey and Robertson*, 2005; *Ulu*, 2009].

For our magnetostratigraphic study of the Aktoprak basin, we sampled 165 levels in ~300 m of stratigraphy. The Kurtulmuş Tepe section is characterized by alternating grey and pink marls, siltstones, claystones, and (less abundant) sandstones. Toward the top, the section is dominated by grey limestones (Figure 2). Carbon and oxygen stable isotope analyses were carried out on samples from the same levels. Additional $\delta^{13}C$ and $\delta^{18}O$ analyses were conducted on 15 samples from the ~50 m long Kızılöz section composed of red and grey sandstones, siltstones and claystones in order to check for temporal changes in paleoenvironment. The Kızılöz section is exposed further up-section from the Kurtulmuş Tepe section, after a stratigraphic gap of ~550 m.

In the following, we present the results of paleomagnetic and rock magnetic analyses, and the results of $\delta^{18}O$ and $\delta^{13}C$ analyses of the lacustrine carbonates. Using the results of these methods along with portable X-ray fluorescence (pXRF) data and scanning electron microscope (SEM) imaging, we aim at (1) determining the paleoenvironmental and tectonic history of the region, and (2) at understanding the various natural processes that produced the current magnetic mineral assemblages, so that we may more accurately interpret the magnetostratigraphy.

2. Paleogeography and Paleoenvironment of Turkey

2.1. Paleogeography of Turkey

The Phanerozoic geologic history of Turkey was characterized by the accretion of Gondwana-derived continental fragments to its southern margin [e.g., *Şengör and Yılmaz*, 1981]. Late Cretaceous to Paleocene collision of the continental Gondwana-derived Anatolide-Tauride Block [e.g., *Tüysüz et al*., 1995; *Kaymakçı et al*., 2009; *Meijers et al*., 2010] and more recently the Eocene to Oligocene collision of Arabia with the southern Eurasian margin were followed by the westward tectonic escape of the Anatolian plate along major strike-slip faults [*Dewey and Şengör*, 1979; *Şengör et al*., 1985]. The tectonic processes associated with Africa-Eurasia collision ultimately led to the formation of the Pontide and Tauride mountain belts and the Anatolian plateau [e.g., *Schildgen et al*., 2014]. The Central Anatolian Plateau (CAP) continues eastward into the



Figure 2. Satellite imagery (copyright DigitalGlobe, Inc.) of the area around the sampled Kurtulmuş Tepe section showing the cyclic red/pink and white bands of the Kurtulmuş Tepe Formation. The black (white) intervals drawn over the sampled section shows the primary normal (reverse) magnetic polarity recorded in the pink rocks.

East Anatolian Plateau (EAP), which sits at a higher average elevation of ~2000 m (Figure 1a). The combined CAP and EAP form the only orogenic plateau in the Eastern Mediterranean region. The Pontide Mountains separate the CAP from the Black Sea in the north, while the Tauride Mountains separate the CAP from the Mediterranean Sea. The topographic evolution of central Anatolia in combination with sea level change resulted in occasional marine incursions interspersed with periods of dominantly continental depositional systems such as lakes and (braided) river systems in Turkey.

There are few quantitative estimates of paleotopography in Anatolia during the Oligocene to Miocene. Oligocene continental clastic deposits [*Krijgsman et al*., 1996; *Jaffey and Robertson*, 2005] in present-day central Anatolia suggest that Anatolia was a topographic high, separating the Mediterranean from the Paratethys domain. Mass flow and alluvial fan deposits in the Oligocene to Early Miocene Ecemiş Basin and the Middle to Late Karsantı basin indicate the presence of some rugged topography [*Jaffey and Robertson*, 2005]. The age constraints on both continental basins are, however, rather limited. Palynofloral elements provide evidence for the existence of moderate paleotopography in Central Anatolia in the Serravalian (Middle Miocene) in the form of mixed-coniferous broadleaved forests [*Akkiraz et al*., 2011], a time during which sedimentation occurred in the continental southwest Anatolian Altinapa basin [*Koç et al*., 2012]. $\delta^{18}O$ data from six paleolake sections in central Turkey suggest there was no orographic barrier from the Late Oligocene (Chattian) to the Late Miocene (Tortonian) [*Lüdecke et al*., 2013; *Mazzini et al*., 2013]. The absence of a significant rain shadow in Central Anatolia prior to the Tortonian [*Mazzini et al*., 2013] is consistent with the results of *Yıldırım et al*. [2011] and *Schildgen et al*. [2012a, 2012b], which indicate that the onset of surface uplift of the central Pontides and Taurides occurred after ~8 Ma. The presence of precisely dated marine rocks at elevations up to 2 km further indicates that surface uplift of the Tauride Mountains postdated the Tortonian [*Schildgen et al*., 2012a,b].

2.2. Paleoenvironment of Anatolia

Paleoclimatic conditions in Anatolia since the Eocene were strongly influenced by overall global cooling following the Early Eocene Climatic Optimum, as well as by the onset of glaciations at the Eocene-Oligocene transition [*Zachos et al*., 2001]. Eocene tropical climate conditions changed to humid subtropical conditions during the Oligocene [e.g., *Akgün et al*., 2002, 2007; *Kayseri-Özer*, 2013]. Temperature reconstructions from

palynoflora analyses indicate that temperatures in Anatolia decreased during the Early Miocene (Chattian and Aquitanian), possibly as a result of Mi1 glaciation [*Kayseri-Özer*, 2013]. Mean annual temperature (MAT) estimates for the Lower and Middle Miocene in central and western Anatolia range from ~16–21°C, with mean coldest month temperatures of ~9 ± 4°C [*Akgün et al*., 2007]. A slightly lower MAT of ~14–17°C for central Anatolia in the Tortonian [*Mazzini et al*., 2013] suggests ongoing cooling. Humid conditions continued into the Miocene, for which mean annual precipitation (MAP) values of 1100–1400 mm/yr (Aquitanian to earliest Tortonian) [*Akkiraz et al*., 2011] or ~900 mm/yr [*Mazzini et al*., 2013], were calculated based on pollen analysis. $\delta^{13}C$ and $\delta^{18}O$ based reconstructions from Oligocene to Miocene central Anatolian lacustrine deposits show a paleoenvironment characterized by large, temporally open lakes in the Late Oligocene. A change toward more arid and closed saline lake conditions occurs approximately in the middle Aquitanian [*Lüdecke et al*., 2013], whereas data from the Tortonian Tuğlu Formation suggest humid, open lake conditions [*Mazzini et al*., 2013].

3. The Oligocene to Lower Miocene Aktoprak Basin

The continental Aktoprak basin is located north of the Tauride Mountains and to the south of the Ulukışla Anticline (Figure 1). The Tauride Mountains are, for the most part, composed of Paleozoic and Mesozoic marine deposits, as well as ophiolitic nappes, mélanges and olistostromes that formed in the Neo-Tethyan realm. Paleocene to Eocene closure of the Neo-Tethys led to the incorporation of Paleocene and Eocene sedimentary and magmatic rocks into the nappes that currently form the Tauride mountain belt. Here we follow the definition of the Aktoprak basin of *Clark and Robertson* [2002, 2005] and *Jaffey and Robertson* [2005], i.e., the Aktoprak basin encompasses the Oligocene to Lower Miocene continental basin fill. The sedimentary rocks of the Aktoprak basin overlie Maastrichtian-Middle Eocene sedimentary and volcanogenic formations of the Ulukışla basin [*Oktay*, 1982, *Demirtaşlı et al*., 1984, *Clark and Robertson*, 2005]. The contact between the Ulukışla basin and the Aktoprak basin is characterized by a disconformity near the basin depocenter and a (low-angle) unconformity near the basin margins [*Clark and Robertson*, 2002, 2005]. The sedimentary rocks that unconformably cover the Ulukışla and Aktoprak basins are estimated to be of Upper Miocene to Pliocene age [*Ulu*, 2009]. A more precise ostracod-based Pontian age (Messinian, i.e., Upper Miocene) is reported in *Riveline et al*. [1990] and is discussed further below.

In this study, we subdivide the Aktoprak basin sedimentary rocks (i.e., Aktoprak Formation) into two members: the Kurtulmuş Tepe and Kızılöz members. The Kurtulmuş Tepe Member consists of grey, beige, white, pink and red sandstones, siltstones, claystones, marls, conglomerates and dolomites. The limestones – becoming more dominant toward the top of the section – are solely white, grey or beige in color. For simplicity, we classify the analyzed samples as either grey (comprising grey, white, and beige rocks) or pink (comprising pink to red rocks). The conformably overlying Kızılöz Member consists of an alternation of mostly red, green and gray cross-bedded sandstones, conglomerates, mudstones and some limestone intercalations.

Chattian-Aquitanian gastropod and ostracod-based ages were determined for the Kurtulmuş Tepe Member [*Blumenthal*, 1956; *Nazik and Gökçen*, 1992]. However, this member was also assigned a Bartonian (Middle Eocene) age based on the correlation of charophytes [*Riveline et al*., 1990]; this age disagrees strongly with regional stratigraphic relationships and the other two biostratigraphic ages, so we do not consider this age further. No age determinations are available for the Kızılöz Member, nor for the travertine deposits that locally overly the sedimentary rocks of the Kurtulmuş Tepe and Kızılöz members.

The Kurtulmuş Tepe Member is interpreted as a rhythmical calcareous succession that was deposited in an open-lacustrine setting. Observed wave-ripple lamination, fossil leaf debris and interbedded stromatolitic microbial mats are indicative of deposition near the lake margin [*Jaffey and Robertson*, 2005]. The top of the Kurtulmuş Tepe section is dominantly calcareous, and changes abruptly to terrigenous clastic deposits (i.e., the Kızılöz Member). Alternation of sandstones and mudstones/siltstones suggests a braided river depositional system characterized by periods of rapid and reduced E-NE flow toward the Ecemiş Fault (Figure 1a) [*Jaffey and Robertson*, 2005]. Facies evidence indicates that the clastic sediments from the Kızılöz Member are predominantly derived from the Tauride Mountains to the southwest of the Aktoprak basin [*Jaffey and Robertson*, 2005], which indicates that the Tauride Mountains were topographically higher than the Aktoprak basin.

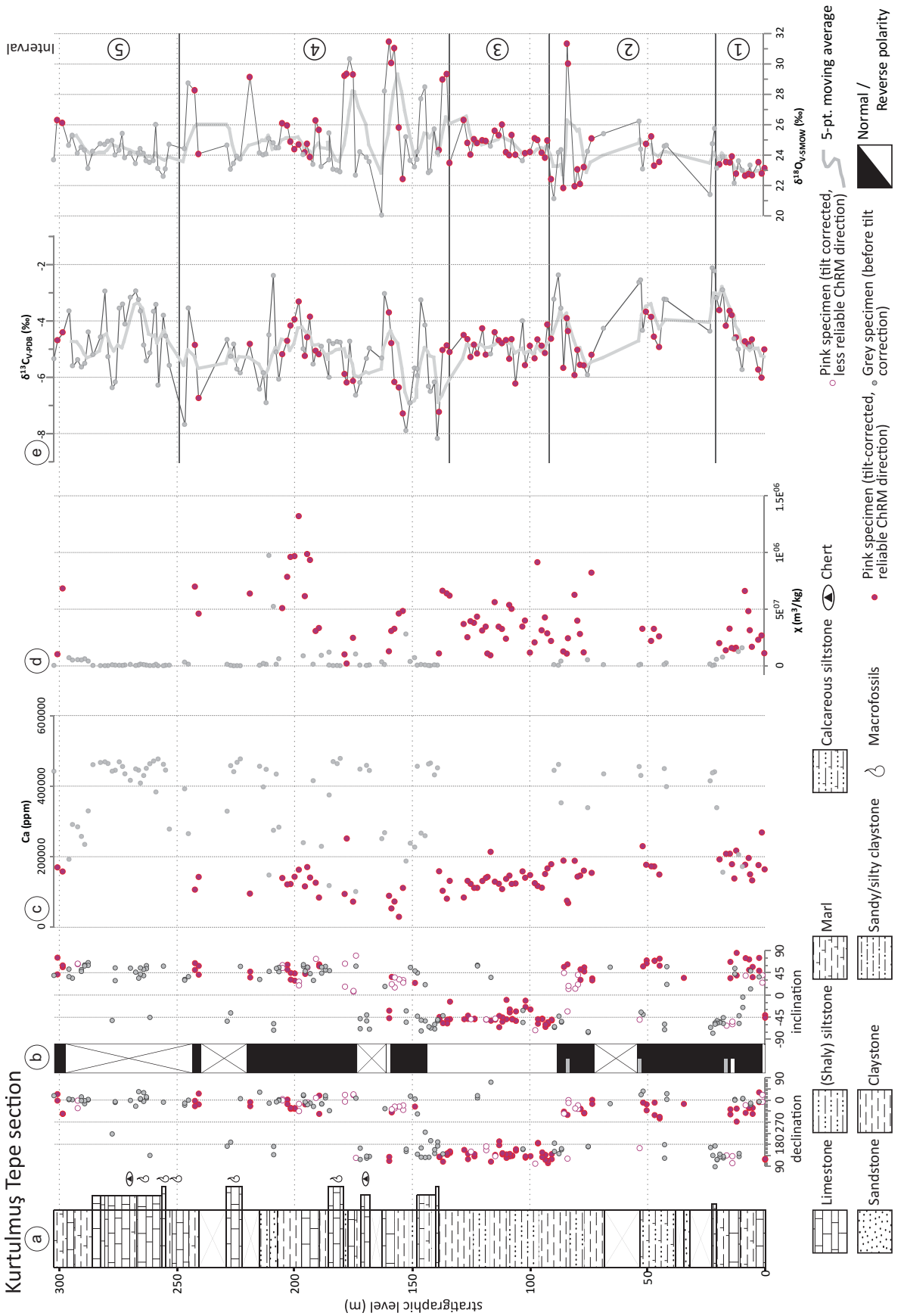

Figure 3. (a) Stratigraphic column of the Kurtulmuş Tepe section. (b) Paleomagnetic results (declination and inclination) for all interpreted specimens. The constructed magnetostratigraphy is solely based on the pink and red sedimentary rocks. Mixed polarity levels are displayed in grey; intervals with no data are crossed. (c) Ca content (ppm) of sampled levels based on pXRF measurements. The Ca content of pink and red rocks is in general much lower than the Ca content of the grey rocks. The Ca content can be directly related to carbonate content (Figure 7j), based on data acquired during stable isotope analysis. (d) Bulk susceptibility data show a distinction between pink/red and grey rocks. Bulk susceptibility is often negative for the grey rocks, which is an indication for the dominant presence of (diamagnetic) carbonate. (e) Carbon and oxygen isotope results for section KL. The results show that there is no relation between the $\delta^{13}C$ and $\delta^{18}O$ values and the color of the rocks.

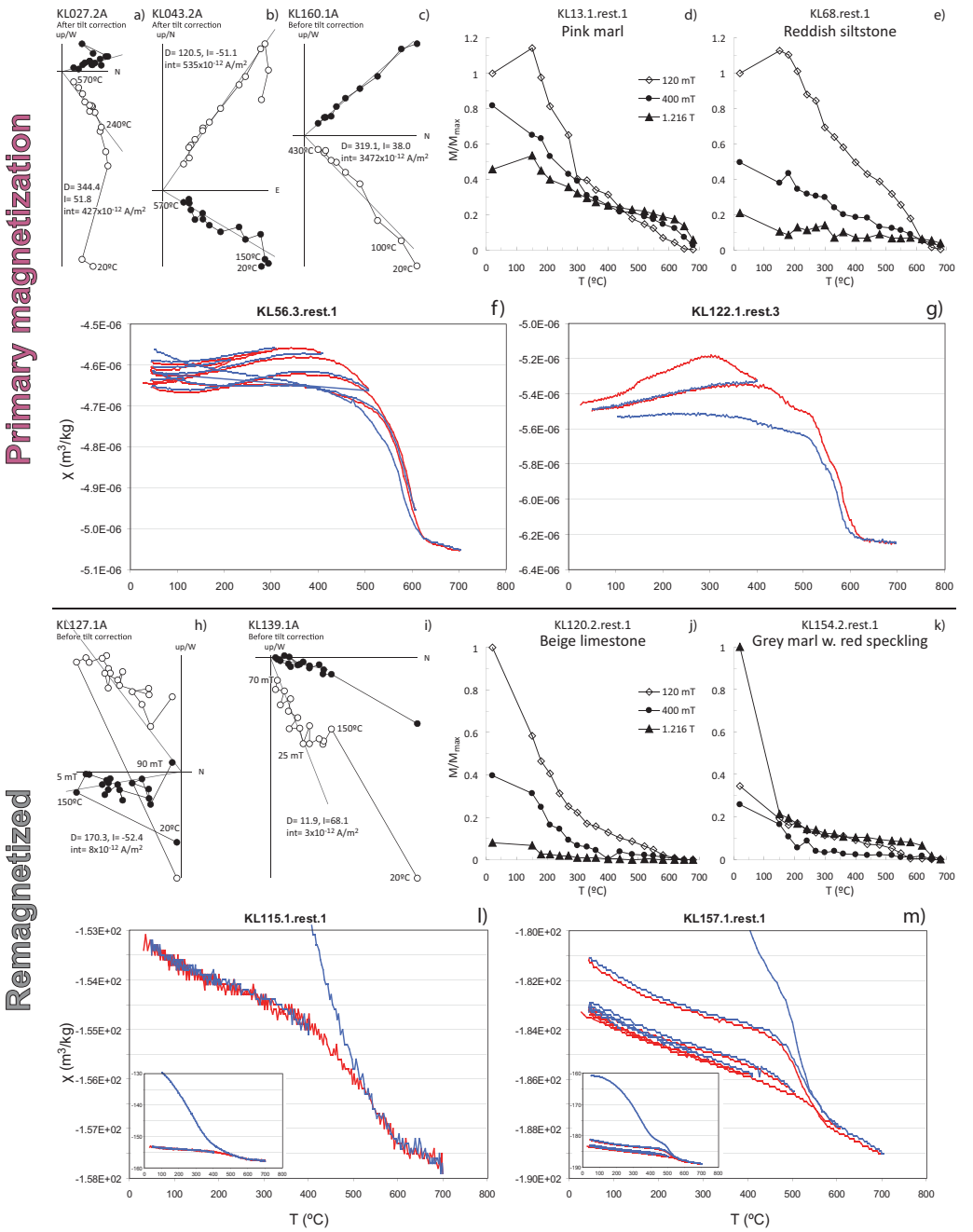

Figure 4. Orthogonal vector diagrams [*Zijderveld*, 1967] showing characteristic demagnetization diagrams for (a–c) the pink rocks and (h, i) the grey rocks. Closed (open circles indicate projection on the horizontal (vertical) plane. Alternating field and temperature steps are indicated. D= declination, I= inclination of the interpreted vector; Int= starting intensity of the NRM. Representative demagnetization diagrams of a composite three-axis IRM for the (d, e) pink and (j, k) grey rocks following *Lowrie* [1990]. Susceptibility versus temperature runs of representative specimens for the f, g) pink (and (l, m) grey rocks.

4. Methods and Results

4.1. Paleomagnetism and Rock Magnetism

4.1.1. Paleomagnetism and Rock Magnetism: Sampling Strategy

Standard paleomagnetic cores (2.54 cm diameter) were collected using a gas-powered motor drill at the Kurtulmuş Tepe section. Three cores were collected at each of the 165 levels over ~300 m of stratigraphy (Figure 3), and the sampling interval corresponds to the lower Kurtulmuş section of *Jaffey and Robertson* [2005]. The orientation of the paleomagnetic cores and the tilt of the beds were measured using a magnetic

compass and corrected for 4.9°E present-day declination. Bedding tilt varies slightly throughout the section (see supporting information), but averages roughly 173/36° (dip direction/dip). Cores were cut into standard paleomagnetic specimens (2.54 cm diameter, 2.20 cm height). Remainders of cores were used for rock magnetic analyses (low temperature experiments and magnetic susceptibility versus temperature runs). Specimens from two out of three cores per level (323 specimens in total) were subjected to either thermal demagnetization (155 specimens) or combined thermal and alternating field (AF) demagnetization (158 specimens). All paleomagnetic and rock magnetic analyses were carried out at the Institute for Rock Magnetism (IRM) at the University of Minnesota. We refer to the time scales of *Vandenberghe et al*. [2012] and *Hilgen et al*. [2012] to correlate the Kurtulmuş Tepe section to the Global Polarity Time Scale (GPTS).

4.1.2. Paleomagnetism and Rock Magnetism: Analyses

All AF demagnetized specimens were first thermally demagnetized to 150°C in order to (1) demagnetize potentially present goethite (Néel temperature = 120°C) [*Özdemir and Dunlop*, 1996] and (2) to remove possible stress on magnetite grains caused by surface oxidation at low temperatures [*Van Velzen and Zijderveld*, 1995]. Initial natural remanent magnetization (NRM) intensities range between ~1 and 10,000 μA/m. NRM demagnetization of representative specimens is displayed in orthogonal vector diagrams [*Zijderveld*, 1967] (Figures 4a–4c, 4h, and 4i). Rocks with higher concentrations of clay minerals (pink rocks) were demagnetized using thermal demagnetization (Figures 4a–4c). More carbonate rich specimens (grey rocks) yielded much lower initial intensities (~1–10 μA/m), and demagnetization diagrams for those specimens show erratic behavior upon thermal demagnetization. The erratic behavior of the low intensity specimens upon thermal demagnetization is possibly due to the effect of chemical alteration during heating, and we therefore used AF demagnetization to recover the magnetization held by this specific group of specimens (Figures 4h and 4i).

Characteristic remanent magnetization (ChRM) directions were determined using principal component analysis [*Kirschvink*, 1980]. Approximately four or five (for the grey rocks) to seven (for the pink rocks) successive demagnetization steps were used to fit a vector. Most specimens carry a low temperature (LT) or low coercive force component (LCF), as well as a high temperature (HT) or high coercive force (HCF) component (Figures 5a–5c, 5f, and 5h). Specimens with overlapping LT/LCF and HT/HCF components were analyzed using the great circle approach (Figures 5a and 5b), to determine the direction that lies closest on the great circle between the two overlapping components and well-determined ChRM directions [*McFadden and McElhinny*, 1988]. All individual components are provided in the supporting information.

Site mean directions, virtual geomagnetic poles (VGPs), and their means were calculated from the ChRM directions [*Fisher*, 1953] (Figures 5a–5c, 5f, and 5h). A fixed 45°-degree cut-off was applied to the VGPs to remove outliers from the calculation of mean directions. The errors in declination (ΔD_x) and inclination (ΔI_x) were calculated following *Butler* [1992]. We favor this approach, since it more realistically describes the increasingly elongated distribution of the directions toward lower latitudes [*Creer et al*., 1959, *Tauxe and Kent*, 2004; *Tauxe et al*., 2008].

Reversal tests were carried out following *McFadden and McElhinny* [1990] and their classification (A, B, C, indeterminate). The classification is based on the critical angle γ_c and the angle γ between the means. This approach uses Monte Carlo simulation and therefore effectively applies the Watson V_w statistic test [*Watson*, 1983].

To correct for possible inclination shallowing, the statistical E/I method was applied [*Tauxe and Kent*, 2004; *Tauxe et al*., 2008] (Figures 5d and 5e). The E/I method is based on the TK03.GAD field model, which in turn is based on the assumption that the Earth's magnetic field averaged over a time interval long enough to average out the secular variation resembles that of a geocentric axial dipole (GAD). The E/I method analyzes the distribution of individual directions and therefore requires the input of a large data set (with N typically >100).

The characterization of magnetic carriers in the rocks was approached using a number of complementary methods. Bulk susceptibility (Figure 3d) at room temperature for one specimen per level was measured in low-field (300 Am^{-1} at a frequency of 920 Hz) using a Geofyzika KLY-2 KappaBridge.

Low temperature experiments (Figure 6) were carried out on specimens (~0.3–0.7 g rock chips) of paleomagnetic cores on a Quantum Designs Magnetic Property Measurement System (MPMS) cryogenic magnetometer (sensitivity 10^{-10} Am^2). The NRM of a number of specimens was measured during low-temperature demagnetization (LTD) of the NRM upon cooling and warming in zero field from room temperature down to 20 K (in some cases 15 K). Specimens are typically given a 2.5 T isothermal remanent magnetization (IRM) prior to experiments in the MPMS to optimize centering of the specimen with respect to the

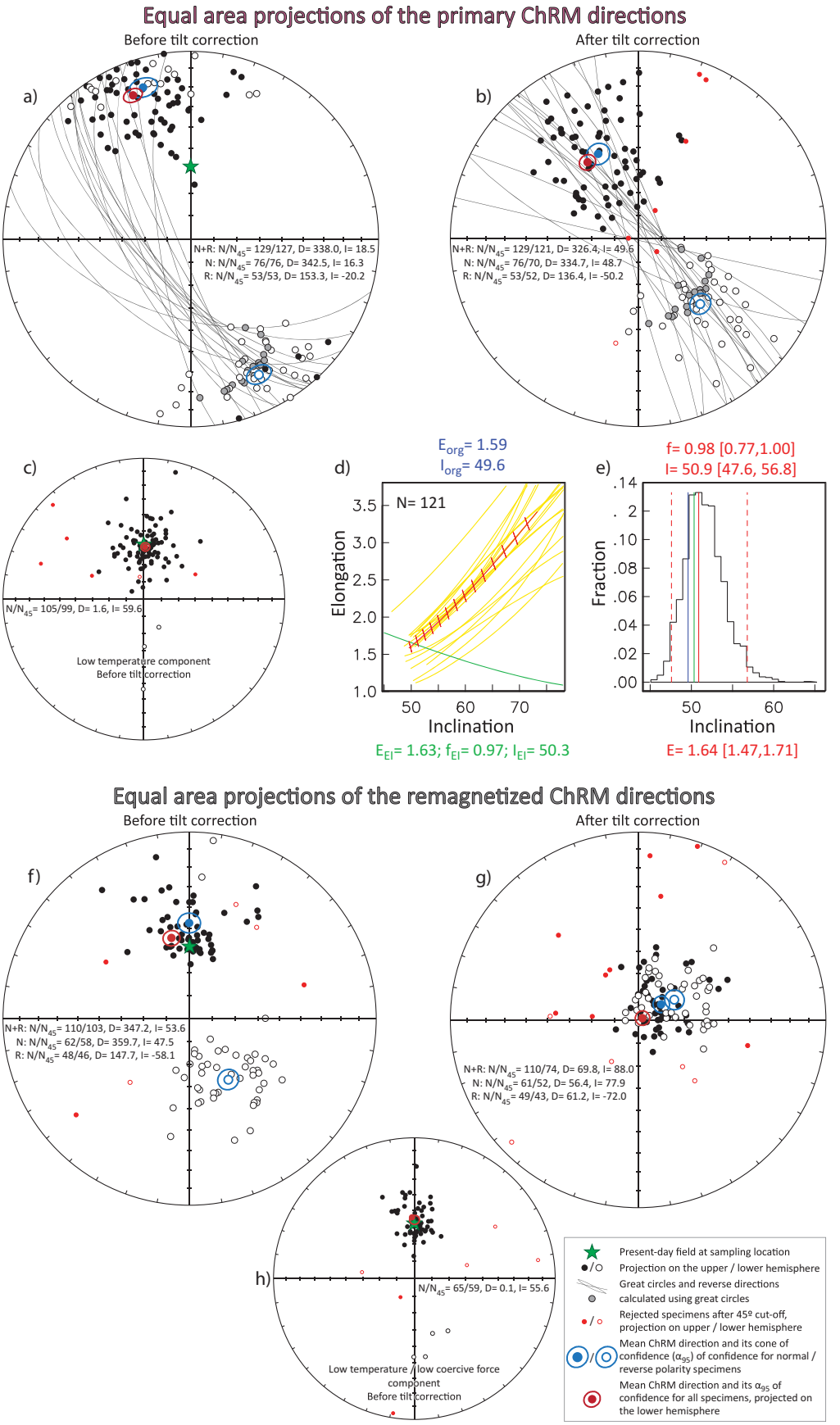

Figure 5. Equal area projections of (a, b, f, g) the individual and mean ChRM directions and (c, h) the low temperature directions. See figure for legend. E/I-correction results after application of the method [*Tauxe and Kent*, 2004] to the primary ChRM directions of the pink and red rocks, with (d) corresponding elongation versus inclination, and (e) fraction (of 5000 bootstraps) versus inclination plots. In Figure 5a, the E/I pair for the TK03.GAD model (green line) and for the data sets (red barbed line) for different degrees of flattening are plotted. The red barbs indicate the direction of elongation (horizontal is E–W; vertical is N–S). Also shown are examples (yellow lines) from 20 (out of 5000) bootstrapped data sets. The crossing points represent the inclination/elongation pair most consistent with the TK03.GAD model, given as inc_{EI} (in green) at the top; inc_{org}= original inclination, E_{org}= original elongation of the data set, E_{EI} and inc_{EI} are the elongation and inclination, respectively. In Figure 5e, a histogram of intersecting points from 5000 bootstrapped data sets is shown. The most frequent inclination (I; solid red vertical line; dashed red vertical lines denote the 95% bootstrap error) is given (with its error range) above the plot; the inclinations of the original distribution (blue vertical line) or the intersection with the model (green vertical line) are indicated; E = the elongation resulting from the bootstrapped data sets. The results of the E/I method are statistically indistinguishable from the original data for this data set and not significant.

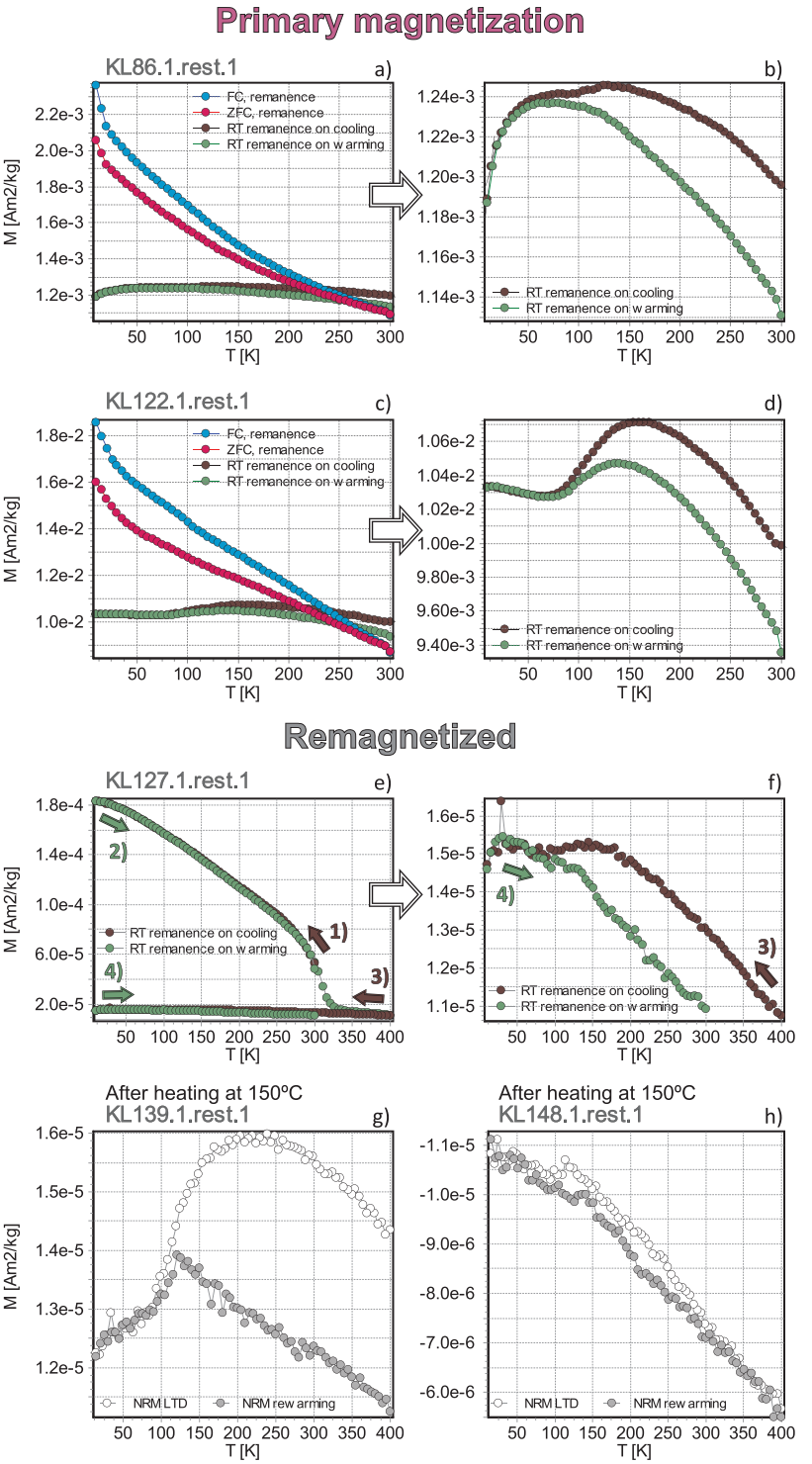

Figure 6. (a, c) Field Cooled (FC) and Zero Field Cooled (ZFC) remanence of an IRM acquired in 2.5 T at 20 K. The specimen is first cooled in a 2.5 T field, after which the remanence is measured upon heating (blue curve), followed by cooling in zero field. After reaching the minimum temperature (20 K), the specimen is given an IRM of 2.5 T and the remanence is measured upon heating (red curve). The experiment is continued by measuring the remanence of a Room Temperature (RT) IRM acquired in a 2.5 T field upon cooling down to 20 K (black curve) and warming up to 300 K (green curve). (b, d) Enlargements of the RT-IRM cooling and warming curves. After the RT IRM experiment in Figure 6e, the specimen was heated up to 400 K (to demagnetize goethite) before repeating the RT IRM experiment. (f) An enlargement of the last RT IRM experiment. (g, h) Low temperature demagnetization experiments of specimens that were initially heated at 150°C to demagnetize goethite.

Table 1. Paleomagnetic Data From the Kurtulmuş Tepe Section Before and After Tilt Correction[a]

Polarity	N_i/N_{45}	D	I	ΔD_x	ΔI_x	k	α_{95}	K	A_{95}
ChRM directions—In situ									
Primary ChRM Directions									
N	76/76	342.5	16.3	3.9	7.3	11.4	5.0	18.6	3.9
R	53/53	153.3	–20.2	3.8	6.9	19.0	4.6	27.7	3.8
N+R	129/127	338.0	18.5	2.7	5.0	14.2	3.4	22.3	2.7
LT/LCF Component									
N+R	105/99	1.6	59.6	4.2	2.8	32.7	2.5	21.0	3.2
Remagnetized ChRM Directions									
N	62/58	359.7	47.5	4.9	5.0	17.1	4.6	20.1	4.3
R	48/46	147.7	–58.1	7.4	5.3	23.0	4.5	14.2	5.8
N+R	110/103	347.2	53.6	5.0	4.2	16.8	3.5	12.5	4.1
LT/LCF component									
N+R	65/59	0.1	55.6	3.9	3.1	46.0	35.7	35.7	3.1
ChRM directions—Tilt Corrected									
Primary ChRM Directions									
N	76/70	334.7	48.7	6.0	6.0	13.4	4.8	11.6	5.2
R	53/52	136.4	–50.2	5.7	5.4	20.2	4.5	17.6	4.8
N+R	129/121	326.4	49.6	4.3	4.2	15.0	3.4	12.8	3.7
Remagnetized ChRM Directions									
N	61/52	56.4	77.9	15.4	3.4	31.9	3.6	11.8	6.0
R	49/43	61.2	–72	12.8	4.5	27.3	4.2	10.8	6.9
N+R	110/74	69.8	88.0	99.9	3.0	28.1	3.2	8.7	5.9
Total number of demagnetized specimens: 313									

[a]Kurtulmuş Tepe −37.522°N, 34.475°E. N= normal polarity, R= reverse polarity, Ni/N45= number of specimens from which a direction has been interpreted/number of specimens after application of a 45° fixed cut-off on the VGPs, D= declination, I= inclination, ΔD_x= declination error, ΔI_x= inclination error, k= estimate of the precision parameter determined from the ChRM directions, α_{95}= cone of confidence determined from the ChRM directions, K= precision parameter determined from the mean virtual geomagnetic pole (VGP) direction, A_{95}= cone of confidence determined from the mean VGP direction, LT= low temperature, LCF= low coercive force.

superconducting quantum interference device (SQUID). Most specimens were, however, heated at 150°C prior to the experiment to demagnetize goethite, and therefore not given an IRM. During Field Cooled–Zero Field Cooled (FC-ZFC) experiments, specimens were cooled from room temperature (RT) to 20 K, first in a 2.5 T field and then in zero field (ZF). Each time the specimen reached the lowest temperature of the experiment (20 K), a 2.5 T IRM was given. The magnetization of specimens was subsequently measured on warming to room temperature (RT) in zero field. This was followed by running a room temperature saturation isothermal remanent magnetization (RTSIRM) experiment, after imparting a 2.5 T IRM on each specimen at room temperature. Measurements of the magnetization were obtained upon cooling to 20 K and subsequent warming to 300 K (both in zero field). No frequency-dependence of susceptibility (neither in-phase nor out-of-phase) was detected in the specimens at room temperature on a Magnon Variable Frequency Susceptibility Meter (frequencies ranged from 100 Hz to 10 kHz). Therefore, frequency-dependent susceptibility measurements as a function of temperature were not carried out using the MPMS.

Magnetic susceptibility as a function of temperature (K/T curves; Figures 4f, 4g, 41 and 4m) was measured using a MFK1-FA Susceptibility Bridge with CS4 Furnace (Agico; 200 Am^{-1} and 976 Hz). Approximately 0.2–0.8 g of powdered rock was heated in air and/or in Argon up to successively higher temperatures (max. 700°C) to monitor possible chemical alteration of the magnetic minerals. Experiments performed on the same specimens in air and in Argon resulted in near-identical results. Based on the K/T curves, Curie temperatures were determined following *Fabian et al*. [2013].

Thermal demagnetization of a three-axis isothermal remanent magnetization (IRM) [*Lowrie*, 1990] was carried out on 23 pristine specimens (Figures 4d, 4e, 4l, and 4m). Prior to thermal demagnetization, an IRM was given to the specimens in three orthogonal directions (1.216 T, 400 mT and 120 mT, respectively) using a 2G pulse magnetizer.

4.1.3. Paleomagnetism and Rock Magnetism: Results

4.1.3.1. Pink, Clay-Rich Sedimentary Rocks

A low temperature (LT) component could be isolated between ~20°C and 150–270°C in most of the pink and red marls, siltstones, claystones and sandstones (Figures 4a and 4b). The LT component is reverse in a small number of specimens (N= 3), which may suggest acquisition of the LT component in these specimens

prior to the last reversal (Brunhes-Matuyama, ~780 ka ago) [*Channell et al.*, 2010]. After applying a fixed 45° cut-off on the VGPs, the LT component (N= 99) is D= 1.6°, I= 59.6° in geographic coordinates (Figure 5c and Table 1). Given that the sampling location did not experience much northward motion since the last reversal, we compare the LT component to the present-day field (D= 0°, I= 57°), and conclude that the LT component must be of relatively recent origin, yet possibly older than ~780 ka. A high temperature (HT) ChRM direction could be isolated in most specimens (129 out of 155) between ~150–270°C and 530–570°C, and occasionally up to only ~430°C (Figures 4a–4c). The HT component carries both normal (N= 76) and reverse (N=53) polarities. After applying a fixed 45° cut-off on the VGPs of the HT component, the mean ChRM direction (N= 121) after tilt correction is D= 326.4°, I= 49.6° (Figure 5b and Table 1). The mean ChRM direction (N= 127) in geographic coordinates is D= 338.0°, I= 18.5° (Figure 5a and Table 1). The means of the normal and reverse polarity high temperature components do not pass a reversal test (γ= 12.0 > γ_c 6.6). The rejected reversal test is likely due to incomplete removal of the LT component in the reverse specimens, which leads the reverse HT component to lie on great circles between the HT and LT components.

The E/I method results (after applying a 45° degree cut-off to the VGPs of the HT component) show a slight—though statistically insignificant—increase of the inclination from 49.6° to 50.9° (lower bound 47.6°, upper bound 56.8°) (Figures 5d and 5e).

Thermal demagnetization of three-axis IRMs shows the soft (120 mT) component demagnetizing fully by ~630–650°, while the two harder components (400 mT and 1.216 T) demagnetize at a slightly higher temperature (680°C; Figures 4d and 4e). The apparent increase in remanence after the 150°C step in Figures 4d and 4e is likely due to loss of remanence held by goethite, which may have been oriented roughly antiparallel to the 120 mT IRM direction. The soft component is likely carried by magnetite and maghemite, whereas the two harder components are carried by various grain size fractions of hematite. Hematite does not, however, carry the ChRM.

Bulk susceptibility of the pink and red rocks shows values between 1.7×10^{-8} and 1.3×10^{-6} m^3/kg, with a median value of 3.2×10^{-7} m^3/kg (Figure 3d). Susceptibility as a function of temperature measurements shows an inversion of maghemite to hematite around 350°C (Figures 4f and 4g). A Curie temperature of 600°C (Figure 4) also indicates the presence of maghemite. Curie temperatures of 580°C and 540°C (Figure 4g) indicate the presence of magnetite, as well as magnetite with cation substitution (likely Ti).

The RT-SIRM measurements (Figures 6b and 6d) show inflection points at ~120 K and separation of cooling-warming curves at ~100 K. The inflection at ~120 K is indicative of the Verwey transition (T_v) in magnetite, while the separation of cooling-warming data near 100 K suggests partially oxidized magnetite (maghemite). The gradual and subdued T_v in the RT-SIRM curves is also an indication of the presence of oxidized magnetite. The decrease in magnetization on the order of ~5% at room temperature before and after cooling the specimen through the Verwey transition also indicates that the amount of stoichiometric magnetite is very small, i.e., most of the magnetization is carried by oxidized magnetite or maghemite. The separation of the FC and ZFC curves all the way up to room temperature is consistent with the presence of goethite (Figures 6a and 6c). The first derivative of the FC-ZFC curves of specimen KL122 (not shown) shows an increase in magnetization at ~260 K across the Morin transition (T_m= 262 K), which indicates the presence of some hematite. While not as strong as the magnetization associated with magnetite/maghemite, the presence of goethite and hematite signals in the low temperature MPMS data is consistent with the results from the thermal demagnetization of a three-axis IRM.

4.1.3.2. Grey, Carbonate-Rich Sedimentary Rocks

In the grey rocks, an LT component can be identified between 20°C and 150°C in approximately half of the demagnetized specimens (Figures 4h and 4i). The LT component (N= 59, D= 0.1, I= 55.6; Figure 5h and Table 1) lies very close to the present-day field direction and is in some cases of reverse polarity (N= 4). This suggests that the LT component in the grey specimens was partially acquired prior to the last geomagnetic reversal, as in the pink rocks. A significant number of specimens with very low NRM intensities behaved erratically upon AF demagnetization (48 out of 158), and no high coercive force (HCF) component could be identified in those specimens. The HCF component in the remainder of the specimens, which we interpret as the ChRM, yields normal (N= 61) as well as reverse (N=49) polarities. The mean HCF ChRM direction after application of a 45° fixed cut-off on the VGPs (N= 103) in geographic coordinates is D= 347.2°, I= 53.6°, which after tilt correction becomes D= 69.8°, I= 88.0° (N= 74; Figures 5f and 5g and

Table 1). An inclination of 88° – corresponding to a paleolatitude of 86°N—is unrealistically high, whereas the mean HCF ChRM directions before tilt correction yield more realistic paleolatitude values for Oligocene-Miocene and younger ages at the study location (the expected inclination between 30 and 20 Ma is $\sim 54 \pm 3°$, following the Eurasian apparent polar wander path of *Torsvik et al*. [2012]). We therefore conclude that the HT ChRM directions for the grey rocks are remagnetized. A reversal test after applying a 45° cut-off on the normal and reverse polarity directions and before tilt correction is negative ($\gamma = 21.8 > \gamma_c$ 6.1). As for the pink and red rocks, we suspect that the negative reversal test results from overlapping LT and HT components, leading the HT directions to fall along the great-circle between the LT and HT components.

All three components of the three-axis IRM experiments are demagnetized by 580°C in most specimens (Figure 4j), suggesting the absence of hematite in these rocks. Evidence for the presence of goethite is indicated by a significant decrease of the hard (1.216 T) component after heating up to 150°C (Figures 4j and jk). The grey marls of specimen KL154.2 display some visible red speckling. The hard component of the three-axis IRM of KL154.2 can only be demagnetized at 680°C (i.e., the Néel temperature of hematite; Figure 4k), and therefore indicates the presence of some hematite. The NRM can be mostly demagnetized using AF demagnetization up to 90 mT, and is therefore mostly carried by magnetite. This is further indicated by the full demagnetization of the soft (120 mT) and medium (400 mT) components at a temperature of 580°C (i.e., the Curie temperature of magnetite).

Bulk susceptibility of the grey rocks ranges between -3.4×10^{-9} and 9.7×10^{-7} m^3/kg, with a median value of 6.6×10^{-9} m^3/kg (Figure 3d). Susceptibility versus temperature runs show Curie temperatures slightly below 580°C (Figures 4l and 4m), which may result from cation-substituted magnetite. As for the pink rocks, we suspect that titanium is the cation that was substituted for magnetite in order to form titanomagnetite (see scanning electron microscopy results below).

Magnetizations in the RT-SIRM experiments show a ~350% increase when cooling the specimen from room temperature to 15K (path 1, Figure 6e), resulting from the spontaneous magnetization of goethite in zero field. After demagnetizing the specimen up to 400K (above the Néel temperature of goethite, 120°C or 393K), the effect of spontaneous magnetization is significantly smaller upon recooling the specimens to 15K (curve 3, Figure 6f). The enlarged view of the RT-SIRM warming and cooling curves after the 400K treatment (Figure 6f) also shows a clear T_v at 120 K and the separation of the two curves occurring between 100 K and 120 K, which suggests that some of the magnetite is partially oxidized. Low-temperature demagnetization of specimens heated to 150°C prior to MPMS experiments display similar behavior.

4.1.3.3. Magnetic Polarity Pattern

Owing to the remagnetized nature of the grey rocks, the magnetostratigraphy of the Kurtulmuş Tepe section is solely based on results for the pink and red sampled levels. Three minor gaps of ~10–20 m and one major stratigraphic gap of ~50 m complicate a possible correlation of the magnetostratigraphy to the geomagnetic polarity time scale (GPTS). Except for one ~55 m long, well-constrained reverse polarity interval, all other sampled intervals are predominantly normal. By omitting the upper ~80 m of the section, due to the largely unconstrained polarity of this interval, the section can be subdivided in the following intervals: (1) a predominantly normal interval up to ~88 m, (2) followed by a ~55 m long reverse interval up to ~144 m and (3) a ~75 m long predominantly normal polarity interval up to ~219 m.

4.2. Carbon and Oxygen Stable Isotope Geochemistry

4.2.1. Carbon and Oxygen Stable Isotope Geochemistry: Sampling Strategy

Samples for stable isotope geochemistry were collected at 162 levels that were also sampled for magnetostratigraphy at the Kurtulmuş Tepe section (Kurtulmuş Tepe Member). In addition, 15 levels of grey and red claystones, siltstones and (cross-bedded) sandstones were sampled in a 50 m section (Kızılöz, KZ) through the Kızılöz Member of the Aktoprak Formation after a stratigraphic gap above the Kurtulmuş Tepe section. The KZ section corresponds to the lower part of the middle Kızılöz section as studied by *Jaffey and Robertson* [2005]. Based on satellite images and the interpolation of measured bedding planes on each side of the stratigraphic gap, the unsampled interval covers 500–600 m in thickness.

4.2.2. Carbon and Oxygen Stable Isotope Geochemistry: Methods

Whole-rock sample powders were digested in orthophosphoric acid and analyzed as CO_2 in continuous flow mode using a Thermo MAT 253 mass spectrometer interfaced with a Thermo GasBench II at the Joint Goethe University—BiK-F Stable Isotope Facility, Institute of Geosciences, Goethe University Frankfurt.

Analytical procedures follow *Spötl and Vennemann* [2003]. Raw isotopic ratios were calibrated against a Carrara marble in-house standard and against NBS18 and NBS19 carbonate reference materials. Final isotopic ratios are reported against Vienna Standard Mean Ocean Water (V-SMOW) for $\delta^{18}O$ and Vienna Pee Dee Belemnite (V-PDB) for $\delta^{13}C$. Analytical uncertainties are typically better than 0.10‰ ($\delta^{18}O$) and 0.07‰ ($\delta^{13}C$). Carbonate contents were derived from standard-sample total peak area ratios and are precise to within 10% absolute. All samples contain at least 24 wt.% carbonate. Results from 177 specimens are given in the supporting information.

4.2.3. Carbon and Oxygen Stable Isotope Geochemistry: Results

4.2.3.1. Kurtulmuş Tepe Section (KL)

Although the $\delta^{13}C$ and $\delta^{18}O$ values derived from the lacustrine carbonates display intervals of changing variability throughout the section (Figure 3e), the overall $\delta^{13}C$ and $\delta^{18}O$ values remain relatively constant throughout the length of the entire section. The mean $\delta^{13}C$ value is -4.9 ± 1.1‰ (1σ standard deviation) and the mean $\delta^{18}O$ value is 24.6 ± 2.0‰ for the ~300 m long section (N= 162). There is no evident covariation between the $\delta^{13}C$ and $\delta^{18}O$ values, except for the interval between 21.3 and 80.8 m. The $\delta^{13}C$ and $\delta^{18}O$ values for the pink and grey specimens do not display different variability (Figure 3e), although the highest $\delta^{18}O$ values (likely resulting from evaporitic conditions) were mostly recorded in the pink sedimentary rocks. The pink sedimentary layers were preferentially sampled however, since they are more likely to yield higher NRM intensities than the grey layers. The observation that the highest $\delta^{18}O$ values were recorded in pink rocks could therefore result from a sampling bias.

The $\delta^{13}C$ and $\delta^{18}O$ variability in the Kurtulmuş Tepe section can be roughly subdivided into five intervals (Figure 3e). The $\delta^{18}O$ and $\delta^{13}C$ values below refer to the means and the 1σ standard deviation for each interval. From 0 to 20.4 m (KL1–KL17; N= 17), the $\delta^{18}O$ values have very low variability at 23.1 ± 0.5‰, whereas the $\delta^{13}C$ values increase from ~–6 to ~–3‰ in the same interval (-4.5 ± 0.9‰). The second interval (21.3–90.8 m; KL18–KL43; N=26) is characterized by increased variability, with $\delta^{18}O = 24.3 \pm 2.3$‰ and $\delta^{13}C = -4.1 \pm 1.2$‰. The third interval (92.4–134.0 m; KL44–KL68; N= 24) displays little variability in $\delta^{18}O$ (24.7 ± 0.7‰) as well as $\delta^{13}C$ values (-4.9 ± 0.5‰) and was mainly sampled in pink sedimentary rocks. The fourth and longest interval (135.2–246.8 m; KL69–KL131; N= 64) shows the highest variability of the entire section, although the mean values for oxygen and carbon stable isotope ratios remain similar ($\delta^{18}O = 25.3 \pm 2.5$‰ and $\delta^{13}C = -5.4 \pm 1.2$‰). The fifth interval (253.3–302.4 m; KL132–162; N= 31), which is dominated by specimens from grey sedimentary rocks, shows a variability in carbon isotopes that is comparable to that of intervals two and four, whereas the variability of the oxygen isotopes is very low and comparable to that of intervals one and three. The mean values remain stable however, at 24.3 ± 0.9‰ and -4.6 ± 1.0‰ ($\delta^{18}O$ and $\delta^{13}C$, respectively).

4.2.3.2. Kızılöz Section (KZ)

Fifteen samples were taken from ~50 m of stratigraphy at the Kızılöz section, which was deposited conformably atop the Kurtulmuş Tepe section (KL) and is exposed after a ~500–600 m stratigraphic gap (Figure 1b). The sampled specimens were red and in a few cases grey clastic rocks (sandstone, siltstone, clayey siltstone), and isotopic results are remarkably similar to those of section KL. The variability of the sampled interval is comparable to that of the third interval of KL, and thus relatively low for $\delta^{18}O$ as well as $\delta^{13}C$ (Figure 9). The mean values with associated standard deviations are: $\delta^{18}O = 24.0 \pm 0.9$‰ and $\delta^{13}C = -4.4 \pm 0.5$‰. The similarity between the data from the KL and KZ sections is also illustrated in the $\delta^{13}C$ versus $\delta^{18}O$ diagram in Figure 10.

4.3. Portable XRF Analysis

4.3.1. Portable XRF Analysis: Methods

To further investigate the differences in the magnetization of the pink and grey rocks, bulk geochemical compositions of specimens were measured using a portable X-Ray Fluorescence (pXRF) device. Measurements were performed on even and clean surfaces of paleomagnetic specimens that had been heated to 150°C. The pXRF measurements were carried out using a Niton XL3t, with a geometrically optimized large area drift detector (GOLDD), following the procedures described in *Hayes* [2013]. A small camera in the unit allowed for checking the specimen's surface appearance at the targeted measurement spot. To lower detection limits for light elements, a built-in helium purge was used. The measurement unit has a silver anode x-ray tube (50 kV, 0–200 μA). Readings were taken using the mining mode setting and calibration, corrected by Compton Normalization. Mining mode includes cycles of four filters that optimize for specific element

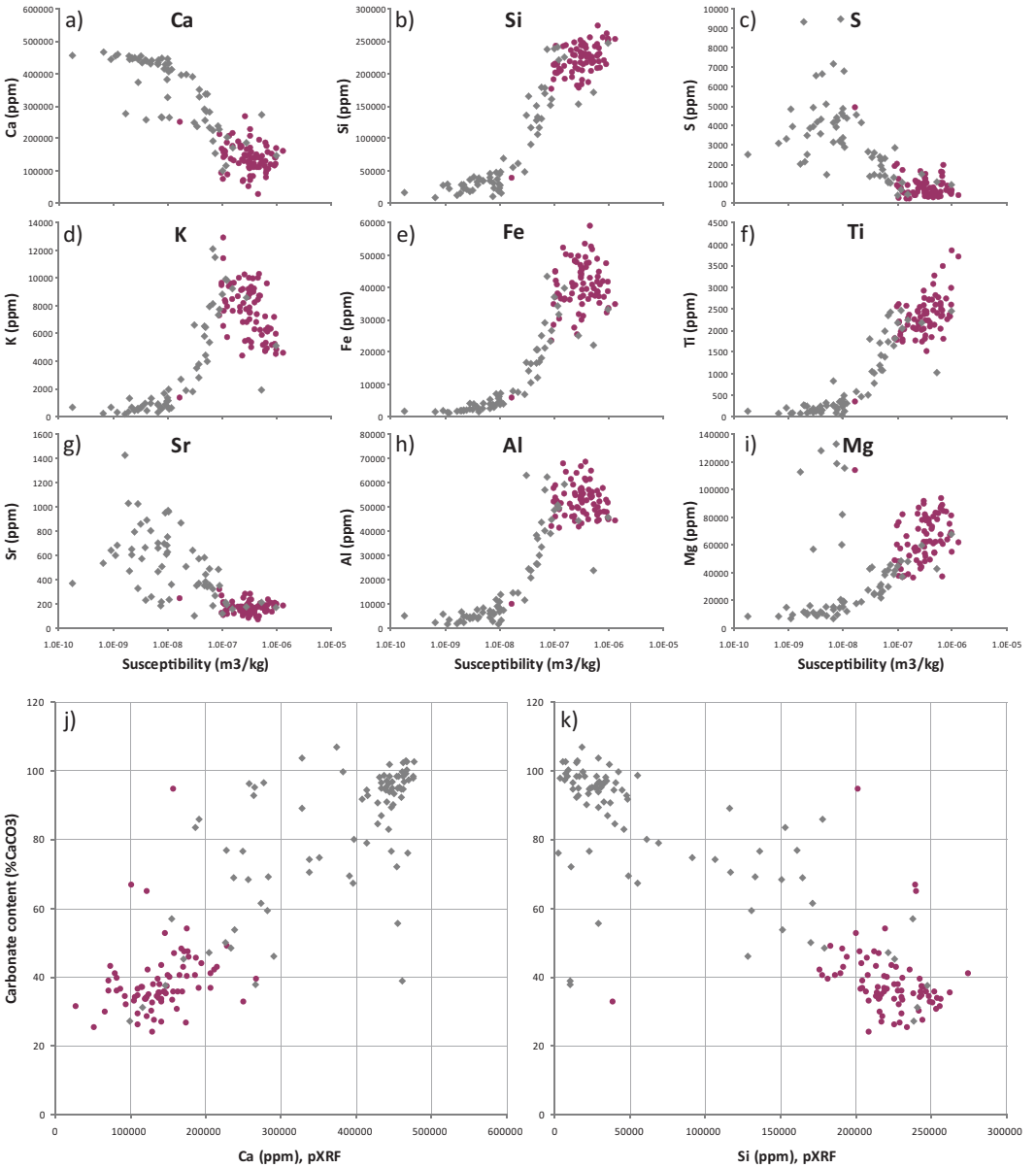

Figure 7. (a–i) Results of the pXRF analysis plotted against the bulk susceptibility for one specimen per sampled level. Carbonate content (determined during stable isotope analysis) plotted versus (j) Ca and (k) Si content (based on pXRF measurements). Ca content increases with increasing carbonate content. The relationship between the carbonate and Ca content shows that most of the Ca in the rocks forms part of carbonate minerals. The inverse relationship between Si content and carbonate shows that Si-content decreases with increasing carbonate content. Pink/red specimens are displayed in pink; grey/beige/white specimens are displayed in grey.

sets by focusing on subsets of the energy spectra. The analyzer assesses over 30 elements, ranging from Mg (lightest) to Bi (heaviest). Each filter was run for 30 s, leading to a total run time of 2 min per specimen. The output of the data is generated in parts per million (ppm) by the analyzer system software. Limits of detection (LOD) are determined by the continuous averaging of detected energy for each analyzed element. Concentrations below 2σ are considered below detection limits. Results for Ca, plotted against the stratigraphy are shown in Figure 3c. Results for selected elements are illustrated in Figure 7. Results for all analyzed elements can be found in the supporting information.

4.3.2. Portable XRF Analysis: Results

pXRF results show a strong correlation between rock color and composition. Pink, clay-rich sedimentary rocks yield overall higher Si, K, Fe, Ti, Al and Mg contents, whereas grey, carbonate rich rocks yield higher Ca, S and Sr contents (Figures 7a–7i). Diagrams showing the elemental composition of the rocks versus stratigraphic level do not reveal any observable cyclicity (e.g., Figure 3c). The positive correlation between

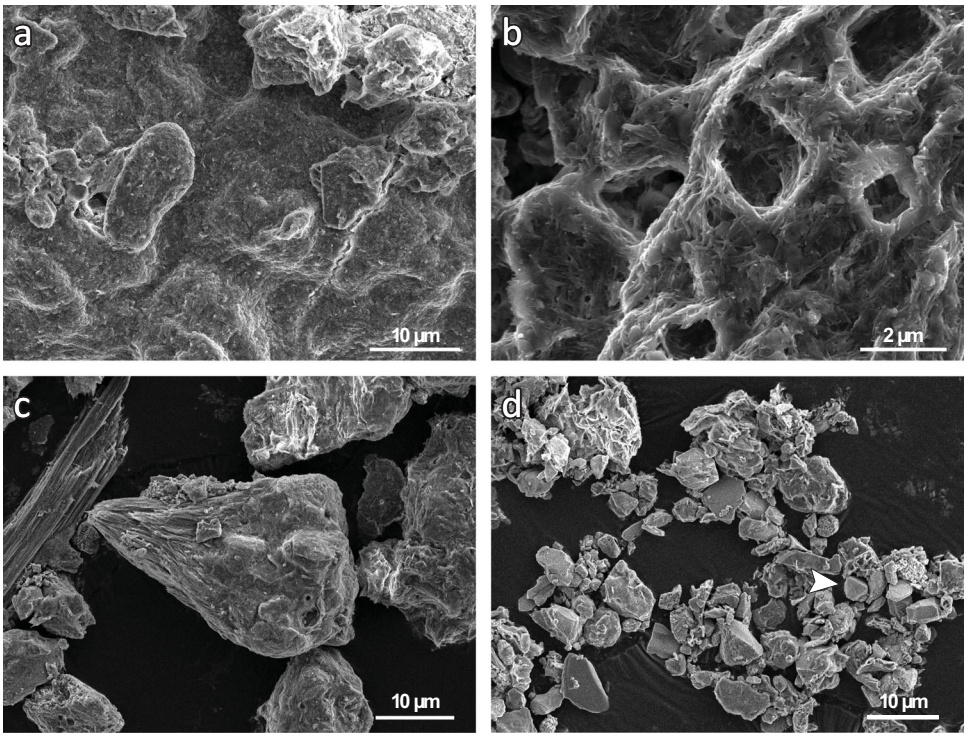

Figure 8. Representative SEM images of magnetic separates from pink, clay-rich samples a) KL 56.3R, b) KL 85.3R, and c) KL 122.1R, and grey, carbonate-rich sample d) KL 157.1B. (a, b) Mats of clay flakes and needle-shaped grains drape on top of larger grains. The magnified view in (b) provides the clearest view of the needle-shaped grains. (c) Larger grains partially covered by needle-shaped grains and clay flakes. Covered regions show relative Fe enhancement in EDS. (d) Blocky grains typical of extracts from grey layers. Arrow indicates octahedral Fe-rich grain consistent with magnetite. Note that average grain size in the grey sample is smaller than in separates from pink layers (Figures 8a and 8c).

Ca and carbonate content (%) as measured during stable isotope analysis (Figures 7j and 7k) suggests that Ca content is a direct indicator of carbonate ($CaCO_3$) content. The negative correlation between Si and carbonate content (%) is therefore likely a direct indicator of the amount of silicate in the sampled rocks. This is further confirmed by the elevated Ti, Al, Mg and Fe contents, which are generally higher in silicates than in carbonates. The pXRF results most importantly provide a clear geochemical difference between the pink rocks that managed to preserve their primary magnetization and the grey rocks that were largely remagnetized.

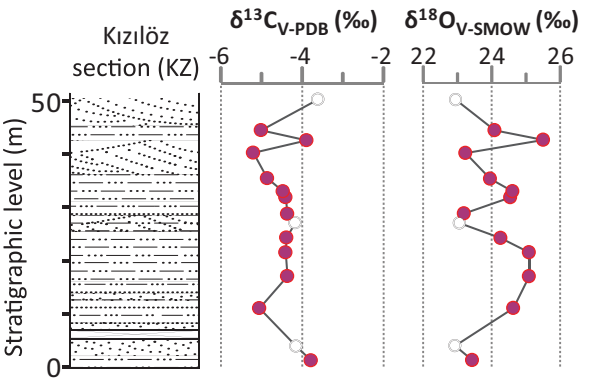

Figure 9. Stratigraphic column and stable isotope results for the red and grey sandstones, siltstones, and claystones of the Kızılöz section (see Figure 3 for legend).

4.4. Scanning Electron Microscopy

4.4.1. Scanning Electron Microscopy: Methods

To characterize the magnetic minerals in the rocks, SEM imagery and energy dispersive spectra (EDS) were obtained. Magnetic separation of ~5 g of powdered rock was conducted following the methods of *Strehlau et al.* [2014]. After dissolution of the carbonate matrix, the remaining components were separated into nonmagnetic components, including any material that was not removed during dissolution, and magnetic extracts. Extracts were deposited dripwise onto carbon tape for imaging. Magnetically extracted particles were characterized using a JEOL 6500 SEM. Samples were prepared by

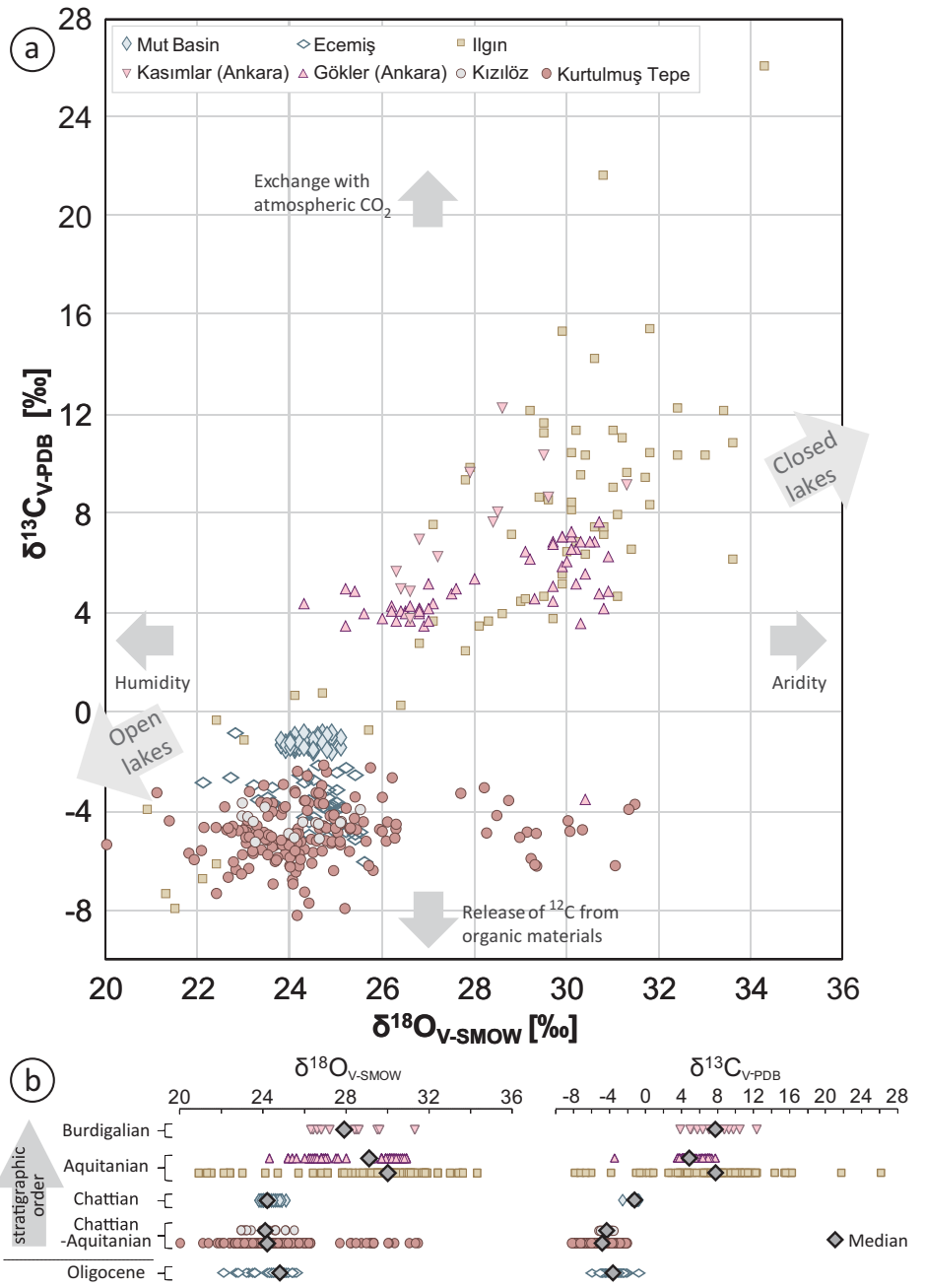

Figure 10. Results of the stable oxygen and carbon isotope analysis. (a) $\delta^{18}O$ versus $\delta^{13}C$ values of all specimens from the Kurtulmuş Tepe and Kızılöz sections, as well as all data from a study by *Lüdecke et al.* [2013]. A covariance between $\delta^{18}O$ and $\delta^{13}C$ may indicate hydrologically closed lakes [*Leng and Marshall*, 2004]. (b) Chart displaying all oxygen and carbon isotopic values our Kurtulmuş Tepe and Kızılöz sections, as well as the results from *Lüdecke et al.* [2013]. The diamonds indicate the median values for each section.

allowing one drop of material to dry on a 12 mm^2 of carbon tape (SPI Supplies, Structure Probe, Inc.) followed by coating with 50 Å of carbon. Energy dispersive spectroscopy (EDS) was conducted using a Thermo-Noran Vantage system for elemental analysis. We cannot readily calculate exact elemental abundances using the EDS data, due to the absorption effects of heavy metals (e.g., iron and titanium), but elemental ratios between metals are usually more dependable and can be interpreted in a qualitative manner. The SEM images (Figure 8) were altered only by linear adjustments to contrast and brightness across each image, in order to use the full range of grayscale values. All microscopy was conducted at the Characterization Facility in the College of Science and Engineering at the University of Minnesota.

4.4.2. Scanning Electron Microscopy: Results

Upon magnetic separation, the grey samples yielded a smaller volume of magnetic extracts than pink samples. Grain size was observed to cover a broad range (<1 μm to 100s of μm) in the magnetic extracts from pink samples, whereas grey samples showed a narrower grain size range with a smaller average diameter based on the total population of extracts (Figure 8). Pink layer extracts were dominated by mats composed of insoluble clay flakes and small (typically 500 nm to 1 μm long) needle-shaped grains, which together coated the surfaces of larger grains. The dimensions of the needle-shaped grains precluded EDS analysis of their composition, but possible candidates for this mineral include goethite, alunite, or gypsum. EDS measurements of the clay-needle mats revealed elevated concentrations of iron. These mats were likely included in the magnetic separation due to the presence of submicrometer iron oxides that are electrostatically bound to clay grains [e.g., *Galindo-Gonzalez et al*., 2009]. By contrast, the magnetic extracts from grey rocks did not contain comparable needle-and-clay mixtures, and instead exhibited a "cleaner" view of iron oxide grains during secondary imaging (Figure 8d). Octahedral grains (occurring in both the grey and pink samples) identified as Ti-rich iron oxides through EDS are likely to be titanomagnetite, which is consistent with the Curie temperatures observed in the bulk samples. The morphology of the octahedral grains (both magnetite and titanomagnetite) does not show any shrinkage cracks related to maghemitization or obvious alteration or dissolution.

5. Discussion

5.1. Paleomagnetic and Rock Magnetic Results

5.1.1. Pink, Clay-Rich Sedimentary Rocks

The combination of the paleomagnetic results—showing a ChRM of pretilting origin—and the rock magnetic results leads us to conclude that the HT ChRM component in the pink, clay-rich sedimentary rocks is of primary origin. The magnetization in the rocks is carried by (titano-)magnetite and maghemite (Figures 4–6). The sampling location was part of the Eurasian plate during the formation of the Aktoprak basin, which gradually moved northward a couple of degrees since the Oligocene. The calculated paleolatitude of 30.4°N (lower bound 26.9°, upper bound 34.3°) is statistically indistinguishable from the expected paleolatitude between 30 and 20 Ma calculated from the apparent polar wander path (34.7°N, lower bound 32.2°, upper bound 37.4°; Eurasian plate) [*Torsvik et al*., 2012]. E/I correction for inclination shallowing is minimal (31.6°N, lower bound 28.7°, upper bound 37.4°; Figure 5), but still statistically indistinguishable from the expected paleolatitude calculated from the apparent polar wander path. The minimal correction for inclination shallowing is not surprising considering the limited northward movement of the Eurasian plate at the study location since the Oligocene. The data suggest that the Aktoprak basin rotated 33.6 ± 4.3° counterclockwise since the deposition of the lacustrine sediments (Table 1). We did not collect measurements of bedding tilt throughout the basin that allow us to correct for the slightly west plunging fold axis of the Aktoprak basin syncline. The correction would likely only be on the order of a couple of degrees and therefore still result in a net counterclockwise rotation. The pink to red color of the rocks is likely due to pigmentary hematite, the presence of which is indicated by the results from the thermal demagnetization of three-axis IRMs and the results from the low temperature magnetometry collected with the MPMS.

5.1.2. Grey, Carbonate-Rich Sedimentary Rocks

The rock magnetic results for the grey rocks show evidence for the presence of goethite and magnetite. Magnetite is likely carrying the ChRM direction in the grey rocks. The inclinations derived from these rocks (after tilt correction) are unrealistically high (88°). The normal and reverse polarity directions of the ChRM in geographic coordinates are close to the present-day field direction at the site. This leads us to conclude that the rocks were remagnetized after tilting. Remagnetization must have occurred over a protracted length of time, because both normal and reverse directions were recorded. The remagnetized rocks recorded slightly shallower latitudes (30.3 < 34.1°N<38.4) than the present-day latitude (37.5°N). Although the calculated paleolatitude is statistically indistinguishable from the present-day latitude, we would expect the remagnetization event to occur at slightly lower paleolatitudes, because of the study location's gradual northward movement over the last ~60 Myrs (~2°, i.e., ~220km since 20 Ma) [*Torsvik et al*., 2012]. Additionally, roughly north-south directed shortening led to folding of the Aktoprak basin. North-south shortening likely occurred over a larger region in Anatolia, and its accommodation potentially added a couple of degrees (110 km of shortening would roughly correspond to 1°) to the northward motion of the Aktoprak basin since its remagnetization.

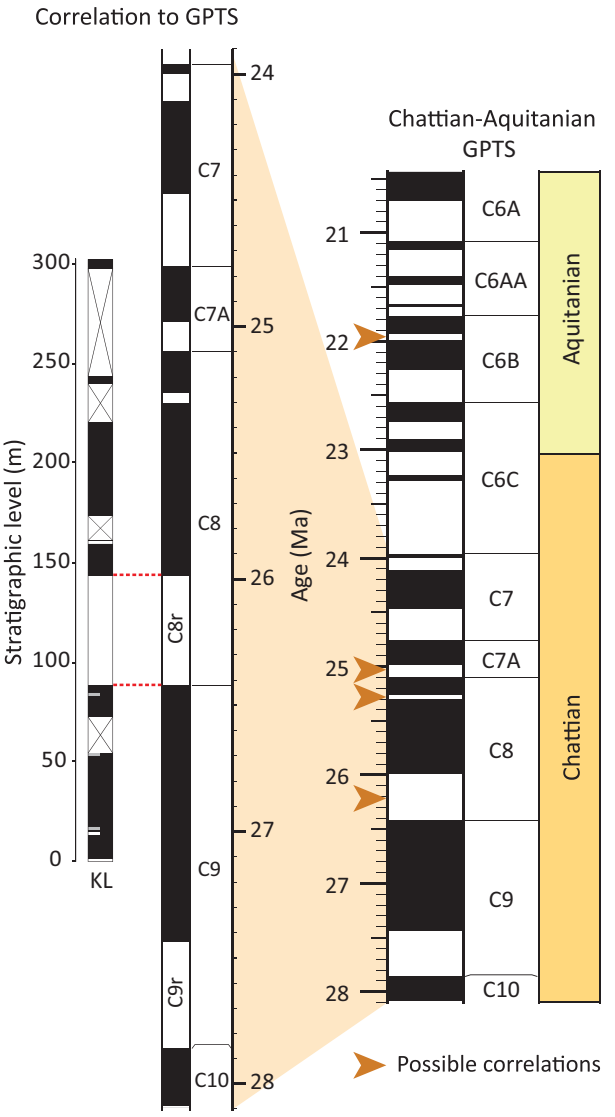

Figure 11. Correlation of the magnetic polarity pattern of the Kurtulmuş Tepe section to the GPTS. Based on the Chattian and Aquitanian biostratigraphic ages [*Blumenthal*, 1956; *Nazik and Gökçen*, 1992] and the length of the individual normal and reverse intervals of the magnetic polarity pattern (derived from the pink sedimentary rocks that carry a primary ChRM), four correlations are possible (right-hand side of the figure). Three of those correlations results in high sedimentation rates that are unlikely for carbonate-rich rocks (see text). Our preferred correlation of the reverse polarity interval to chron C8r is indicated on the left-hand side and leads to a sedimentation rate of 127 m/Myr.

5.1.3. Correlation of the Magnetic Polarity Pattern to the GPTS

The magnetic polarity pattern derived from the pink, clay-rich horizons carrying primary ChRM directions reveals that the lower ~88 m of the section are of normal polarity, followed by a ~55 m reverse polarity interval and a ~75 m long normal polarity interval (Figure 3b). The two short intervals of the upper part of the section (~80 m) that yield results from nonremagnetized, pink sedimentary rocks are of normal polarity. Based on regional stratigraphic relationships and ostracod and gastropod biostratigraphy, the age of the Kurtulmuş Tepe section is bracketed by the Chattian and Aquitanian. Despite the limitations of biostratigraphic age determinations in continental sedimentary settings owing to the isolated nature of continental basins, we attempt to correlate the polarity pattern of our sampled Kurtulmuş Tepe section to the Chattian-Aquitanian GPTS. The ~55 m long reverse polarity interval, preceded and followed by relatively long normal polarity intervals, can potentially be correlated to four polarity chrons (Figure 11). In the Chattian these are the three polarity chrons C8r, Cn.1r and C7Ar. For the Aquitanian, this is polarity chron C6Bn.1r. The corresponding sedimentation rates calculated for a correlation of the magnetic polarity pattern to chrons C8n.1r and C6Bn.1r would be unrealistically high (13,750 and 982 m/Ma, respectively). The sedimentation rates for chrons C8r (127 m/Ma) and C7Ar (478 m/Ma) are somewhat more realistic, although the sedimentation rate for chron C7Ar still seems rather high for carbonate-bearing lacustrine sedimentary rocks. The rocks that recorded the reverse polarities consist of alternating claystones and siltstones, with bed thicknesses varying between 5 cm and 40 cm. We would therefore prefer a correlation to chron C8r, which yields reasonable depositional durations for individual beds between ~300 and 3150 years. Extrapolating the sedimentation rate that results from a correlation to chron C8r for the entire section would result in a ~2.4 Ma sedimentation history (roughly from 27.1 to 24.7 Ma). This age designation would also make the sedimentation history of the Kurtulmuş Tepe section overlap in time with that of the Mut Basin section of *Lüdecke et al.* [2013], which displays strikingly similar $\delta^{18}O$ and $\delta^{13}C$ values compared to this study (Figure 10). Our KL section could possibly cover a larger time span, since it becomes less siliciclastic toward the top of the section and consists of more limestones, which may accumulate at lower sedimentation rates. We note, however, that the correlation we propose above is limited in robustness by the presence of the two unexposed intervals in the first ca. 220 m of the section.

5.2. Timing and Cause of Remagnetization

Based on the directional data, remagnetization must have occurred after tilting of the sampled strata. The remagnetized ChRMs in the grey, carbonate-rich rocks yield normal and reverse polarities, and remagnetization must therefore have occurred over an extended time span. The northward movement of the Eurasian plate at the study location since the deposition of the Aktoprak basin sediments is limited to ~2°. A comparison between the paleolatitude of the remagnetized mean ChRM and the expected paleolatitude from the apparent polar wander path does not provide enough resolution to further constrain the timing of remagnetization. The remagnetized ChRM is close to the present-day field direction and remagnetization could have continued to occur up to the present day. However, the normal and reverse polarities that were recorded in the remagnetized limestones indicate that onset of remagnetization must have occurred before the last geomagnetic field reversal (i.e., Brunhes-Matuyama, ~780 ka ago) [*Channell et al*., 2010].

Terrestrial carbonates are often found to be remagnetized and a variety of mechanisms have been proposed in earlier studies. The recent review of remagnetized carbonates by *Jackson and Swanson-Hysell* [2012] identified two general mechanisms: (1) thermoviscous resetting of magnetic minerals owing to elevated temperatures during burial [*Kent*, 1985], and (2) chemical remagnetization resulting from basinal or orogenic fluid flow, resulting in a chemical remanent magnetization (CRM) [*McCabe and Elmore*, 1989]. Chemical remagnetization is generally thought to preferentially dissolve the submicrometer iron oxide grains that retain primary magnetic recordings and eventually reprecipitate low concentrations of secondary magnetic minerals from the involved basinal fluids [*Jackson and Swanson-Hysell*, 2012]. The quantity of external fluids involved in the remagnetization process is debated, and a number of studies have found that chemical remagnetization may result from ongoing internal cycling of fluids, or involves only limited amounts of externally sourced fluids [*Katz et al*., 1998; *Machel and Cavell*, 1999; *Katz et al*., 2000; *Blumstein et al*., 2004]. Chemical remagnetization may occur in the absence of elevated burial temperatures, in contrast to thermoviscous remagnetization. Because of the large number of marine carbonate rocks that have historically been studied for paleomagnetism (in contrast to lacustrine carbonates), most studies that aimed at understanding remagnetization processes in carbonates have focused on marine carbonates. In order to investigate the nature of remagnetization in the lacustrine rocks of the Kurtulmuş Tepe section, we summarize a number of characteristics of the pink and grey layers below.

Remagnetization in the Aktoprak basin continental sedimentary rocks occurred solely within layers composed of grey, carbonate-rich rocks and not in the interbedded pink, clay-rich layers. The pXRF data show compositional differences between the pink and grey rocks, with grey rocks yielding higher carbonate content than the pink rocks (average $\%CaCO_3 =$ 82% versus 38%, respectively). This indicates that remagnetization of the grey rocks is mineralogically biased toward the carbonates. Upon magnetic separation, grey samples yielded a much smaller volume of magnetic grains than pink samples. Additionally, SEM images show a significant fraction of clay minerals in the magnetic extracts from the pink rocks. Another major difference between the pink and grey layers is their initial NRM intensity, which is on average 1–2 orders of magnitude higher in the pink rocks than in the grey rocks. Based on a combination of paleomagnetic, rock magnetic and SEM data, the magnetic carriers of the ChRM in the pink rocks are likely (titano-)magnetite and (titano-)maghemite, whereas the magnetic carrier of the ChRM in the grey rocks is likely (titano-)magnetite. Below, we investigate the possible mechanisms that could have caused remagnetization of the carbonate-rich grey rocks.

As mentioned above, remagnetization is localized within the grey carbonate-rich layers in the Kurtulmuş Tepe section. One layer may be remagnetized, whereas the surrounding layers may not be remagnetized, depending on their color. Elevated burial temperatures leading to thermoviscous resetting of the magnetic minerals would be unlikely to affect only the grey layers. We therefore think that remagnetization is not caused by thermoviscous resetting. Having omitted a thermoviscous origin for the ChRM, we will further investigate the possibility of chemical remagnetization of the grey layers.

The significant clay fraction in the pink rocks may be an important clue as to what caused remagnetization of only the carbonate-rich grey rocks. The presence of clay particles in the pink rocks likely results in reduced porosity and permeability relative to the grey rocks. Any fluids related to deformation in the Aktoprak basin may have therefore been concentrated along the more permeable grey layers. Fluid flow is commonly associated with remagnetization and can lead to the removal and reprecipitation of magnetic

minerals. Given the low NRM intensity of the grey rocks compared to the pink rocks, fluid flow may have removed a significant portion of the magnetic grains that would otherwise carry a ChRM. The average carbonate content of the pink rocks is approximately half of that of the grey rocks. The remainder of the pink and grey rocks is likely silt and clay-sized detrital input originating from the surrounding rock formations, as evidenced by the octahedral magnetic minerals of inferred igneous origin imaged by SEM. A ~50% smaller input of clastic material into the grey rocks would, however, not explain an on average ~1–2 orders of magnitude lower NRM intensity. It is therefore likely that the low NRM intensities are a result of removal of the original magnetic minerals from the grey layers. Then, in order to carry a post-depositional CRM, new magnetic minerals must have precipitated.

Reprecipitation of new magnetic minerals in remagnetized rocks commonly produces magnetic grains in the superparamagnetic (SP) and stable single domain (SSD) size ranges. Frequency dependence of susceptibility may be a good indicator for the presence of SP particles. However, we did not observe a variation of susceptibility as a function of frequency (100 Hz–10 kHz) at room temperature in either the grey or pink rocks. At first this may seem to suggest that a significant quantity of SP particles is absent in the remagnetized grey rocks. However, the susceptibilities of these grey rocks were so low and were so dominated by diamagnetic carbonates that calculations of room temperature frequency dependence may not have had sufficient resolution and sensitivity to properly identify the presence of SP grains. Additionally, these low susceptibility values make it difficult to deconvolve the susceptibility contributions of the multidomain (MD) (titano-)magnetites imaged using SEM from the contributions of SP and SSD that may have been reprecipitated during the remagnetization process. Given these limitations, in this instance susceptibility does not appear to be a particularly useful tool for characterizing the presence of SP and SSD grains.

Although we have no direct evidence for the precipitation of neo-formed magnetic minerals that carry a CRM, we conclude (based on our observational, rock magnetic, XRF and SEM data) that remagnetization is linked to fluid flow in the basin. Fluids preferentially used the relatively permeable grey layers as pathways (as opposed to the clay-rich pink layers). Fluid flow in the pink, clay-rich layers was sluggish enough to allow for the precipitation of pigmentary hematite, while fluid flow in the grey layers was sufficient enough to remove many of the primary magnetic grains, and eventually to reprecipitate newly formed magnetic grains that carry the remagnetized ChRM. Thus, under the given conditions (i.e., no significant heating of rocks), the neo-formed magnetic minerals that carry the remagnetized ChRM in the grey rocks are likely to be magnetite. Because of the higher solubility of Ca in groundwater relative to Fe, it is unlikely that this fluid-driven process would have led to reprecipitation of new carbonate minerals. Instead, the isotopic values of carbon and oxygen in the grey rocks would be expected to remain relatively unaltered compared to their original values.

5.3. Carbon and Oxygen Stable Isotope Geochemistry

5.3.1. Carbon and Oxygen Stable Isotope Geochemistry on Lacustrine Carbonates

Carbonate minerals such as calcite and aragonite precipitate in most freshwater lakes. Carbonate deposition may result from: (1) concentration through evaporation, (2) biogenic mediation, (3) riverine clastic supply and (4) eolian input [e.g., *Talbot*, 1990; *Gierlowski-Kordesch*, 2010]. Carbonate deposition in relatively dynamic lake environments is typically controlled by three factors: sediment input, hydrology (including water input, output, residence time, balance, origin and composition), and temperature fluctuations [*Gierlowski-Kordesch*, 2010].

The rock record of paleolakes contains valuable information regarding the paleoenvironmental conditions under which the carbonates precipitated. Depending on the hydrological budget, a lake may be classified as open or closed. Closed lakes may be periodically dry, leading to the deposition of evaporites. Provided that authigenic carbonates precipitated in equilibrium with the lake water, carbon and oxygen stable isotope geochemistry may give us important information about lake environments.

The main parameters that influence $\delta^{13}C$ values of lake waters are (1) CO_2 exchange between the atmosphere and total dissolved inorganic carbon (TDIC), (2) photosynthesis and respiration of aquatic plants, and (3) the isotopic composition and physicochemical conditions of inflowing waters, which in turn are influenced by terrestrial plant respiration and metabolism [e.g., *McKenzie*, 1985; *Kelts and Talbot*, 1990; *Talbot and Kelts*, 1990; *Romanek et al.*, 1992; *Leng and Marshall*, 2004; *Gierlowski-Kordesch*, 2010]. C4 plants lead to

the precipitation of approximately 14‰ more positive $\delta^{13}C$ values than C3 plants. By comparison, the effect of temperature on $\delta^{13}C$ during carbonate precipitation is relatively small.

$\delta^{18}O$ values of lake water are also influenced by the composition of inflowing water, but temperature—and by extension evaporation—tends to play a more influential role than for carbon. Evaporation and condensation are the principal fractionation mechanisms for water in the continental hydrological cycle [*Horita and Wesolowski*, 1994]. Authigenic and biogenic carbonates in the rock record that formed from lake water are surmised to reflect changes in inflowing water composition and temperature [e.g., *Leng and Marshall*, 2004].

The (inverse) covariance between $\delta^{13}C$ and $\delta^{18}O$ values in terrestrial carbonates is often used to distinguish between open and closed lake conditions. Inverse covariance (i.e., recording maxima in $\delta^{13}C$ and minima in $\delta^{18}O$ and vice versa) in authigenic carbonates generally results from an increased productivity in a hydrologically open lake setting [*Schelske and Hodell*, 1991], whereas closed lakes are generally characterized by a covariance between $\delta^{13}C$ and $\delta^{18}O$ (i.e., maxima in $\delta^{13}C$ and maxima in $\delta^{18}O$ and vice versa) [e.g., *Li an Ku*, 1997].

For a study of lacustrine sedimentary rocks, it is important to consider the effect of altitude on the $\delta^{18}O$ values of meteoric water. The CAP presently sits at an altitude of ~1000 m and is bound to the north (Pontide Mountains) and south (Tauride Mountains) by orographic barriers with elevations of up to 3000 m. Air masses that are the source of precipitation are forced to higher altitudes along these orographic barriers, leading to a systematic decrease in $\delta^{18}O$ values of precipitation [*Schemmel et al*., 2013]. This change in $\delta^{18}O$ values with elevation ("isotopic lapse rate") across the Pontide and Tauride mountains belts (–2.6‰/km and –2.9‰/km, respectively) [*Schemmel et al*., 2013] is fairly close to the globally averaged lapse rate of –2.8‰/km [*Poage and Chamberlain*, 2001; *Lechler and Niemi*, 2011]. Because precipitation with lower $\delta^{18}O$ values owing to the presence of orographic rainout eventually ends up in lake waters, the development of a rain shadow may be reflected in $\delta^{18}O$ reconstructions of lacustrine sedimentary rocks. In Anatolia, we can observe the emergence of a rain shadow in the significantly lower $\delta^{18}O$ values of Cappadocian Pliocene lacustrine sedimentary rocks [*Göz et al*., 2014] that overlay higher values in Oligocene to Upper Miocene (lower Tortonian) carbonates [*Lüdecke et al*., 2013; *Mazzini et al*, 2013]. These isotopic changes likely reflect the effect of the uplift of the Tauride and Pontide mountain belts after ~8 Ma [*Yıldırım et al*., 2011; *Schildgen et al*., 2014].

Upon the interpretation of our stable isotope data from the Aktoprak basin, we have to bear the variables listed above in mind.

5.3.2. Carbon and Oxygen Stable Isotope Geochemistry of the Aktoprak Basin

To first order, the Kurtulmuş Tepe and Kızılöz data sets (Figure 10) show relatively stable $\delta^{18}O$ and $\delta^{13}C$ values, with some isolated levels in the Kurtulmuş Tepe section characterized by elevated $\delta^{18}O$ values (>~27‰) indicative of evaporitic lake conditions (Figure 3, upper part of interval 2 and interval 4). However, these elevated $\delta^{18}O$ values of the Kurtulmuş Tepe section occur episodically only and are in every case preceded and followed by intervals with $\delta^{18}O$ values that are close to the mean (24.6‰). The intervals of elevated $\delta^{18}O$ values in the Kurtulmuş Tepe section are not restricted to a certain rock color (i.e., pink or grey), which suggests that there is no correlation between rock color and evaporitic environmental conditions. The younger Kızılöz section does not show elevated $\delta^{18}O$ values. The $\delta^{13}C$ values in both the Kurtulmuş Tepe and Kızılöz sections are relatively low, ranging from –8.2‰ to –2.1‰. The combination of relatively low $\delta^{13}C$ and $\delta^{18}O$ values, in combination with the absence of features indicative of evaporative conditions in the stratigraphy suggests that the Aktoprak lake system was hydrologically open. Large water volumes and stable lake levels dominated most of the basin history, with the exception of a small number of short-lived periods during the deposition of the Kurtulmuş Tepe Member that indicate evaporitic and thus more arid conditions.

A previous study of $\delta^{18}O$ and $\delta^{13}C$ isotopes from five Oligocene to Miocene central Anatolian lacustrine carbonate sections [*Lüdecke et al*. [2013] included a review of existing mammal and magnetostratigraphic ages, complemented by $^{40}Ar/^{39}Ar$ ages from volcanic ash layers for two of the five studied sections. The Chattian, Aquitanian and Burdigalian ages of four sections are well-documented. Based on the oxygen and carbon isotopic composition of the Ecemiş corridor section, its age (formerly determined to be Oligocene-Early Miocene) [*Jaffey and Robertson*, 2005] was tentatively assigned to the Chattian.

The correlation of the magnetostratigraphy of the Kurtulmuş Tepe section to the Chattian GPTS relies strongly on the correctness of the biostratigraphic correlation for the Aktoprak basin. The similarity between

the isotopic composition of the well-dated Mut Basin section [*Lüdecke et al*., 2013] and our Kurtulmuş Tepe section (Figure 10) provides an additional argument for placing our sampled section in the Oligocene (Chattian), rather than the Miocene (Aquitanian). The similarity between the isotopic data from our two sections and the data from the Chattian Mut basin and the Ecemiş corridor is remarkable, except for the short-lived episodes of arid conditions in the Kurtulmuş Tepe section. However, the sampled stratigraphic interval of the Mut basin is more condensed and only 9 m long, and if any evaporitic periods occurred during the deposition of the Mut basin fill, these could easily have been so thin as to have been overlooked. The isotopic compositions for three Lower Miocene lacustrine sections from the wider Central Anatolian Plateau region reported by *Lüdecke et al*. [2013] indicate a transition from a subtropical, humid Late Oligocene climate toward arid conditions in the Early Miocene (late Aquitanian), consistent with the development of increasingly closed lake systems.

Oxygen isotopic compositions of lacustrine carbonates commonly reflect the composition of lake water ($\delta^{18}O_{lw}$) during carbonate precipitation [e.g., *Leng and Marshall*, 2004]. $\delta^{18}O_{lw}$ values can be reconstructed using temperature-dependent carbonate-water fractionation equations [e.g., *Kim and O'Neil*, 1997]. However, temperature is not the only variable that determines the $\delta^{18}O_{lw}$, and a temperature change of 14°C in lake water would only lead to a 3‰ change in $\delta^{18}O$ of the formed carbonate. By assuming a range of lake water temperatures ($T_{lw} = 17 \pm 7$°C), we can calculate the corresponding $\delta^{18}O_{lw}$ values from which the sampled carbonates must have precipitated. This will allow us to compare the $\delta^{18}O_{lw}$ values to the $\delta^{18}O$ values of modern meteoric water ($\delta^{18}O_{mw}$) in the study region [*Schemmel et al*., 2013]. Modern $\delta^{18}O_{mw}$ values reflect the rain shadow that is created by the presence of the Tauride Mountains orographic barrier to the south. Isotopic lapse rates across the Tauride Mountains are currently –2.9‰/km, leading to a change of $\delta^{18}O_{mw}$ values of up to ~8‰ across the mountain range [*Schemmel et al*., 2013]. $\delta^{18}O_{mw}$ values around our study area are ca. –10.7‰ (N = 7) [*Schemmel et al*., 2013]. Based on our mean carbonate $\delta^{18}O = 24.6$‰ value for the Kurtulmuş Tepe section (the value for the Kızılöz section is comparable at 24.0‰), the $\delta^{18}O$ values of lake water from which the carbonates precipitated is -5.2 ± 1.5 ‰ (for $T_{lw} = 17 \pm 7$°C).

The calculated values for the Chattian lake waters of the Aktoprak basin are therefore 5.5 ± 1.5 ‰ more positive than the values of modern meteoric waters. The more positive values may be due to (1) the effect of evaporation on the Oligocene lake waters, or (2) the absence of an orographic barrier. The evaporative signal in the isotopic data for the KL and KZ section is limited to isolated horizons within the stratigraphy. This suggests that the more positive $\delta^{18}O$ values of the lake waters are the result of the absence of a substantial orographic barrier. This conclusion confirms the results of the isotopic study of lacustrine sedimentary rocks by *Lüdecke et al*. [2013] for the Late Oligocene (Chattian) to Middle Miocene (Langhian). Additional isotopic data from lacustrine sedimentary rocks by *Mazzini et al*. [2013] for the Late Miocene (Serravalian) indicate the absence of a rain shadow, consistent with the geological evidence for the onset of uplift after ~8 Ma [*Yıldırım et al*., 2011; *Schildgen et al*., 2012a,b]. Sedimentological evidence for the presence of rugged relief along the Ecemiş Fault (Figure 1b) and in the Karsantı basin [*Jaffey and Robertson*, 2005] seemingly contradicts our conclusion that a substantial orographic barrier was absent in the Late Oligocene. The created topography along the Ecemiş Fault may, however, result from fault activity and be relatively low and localized. The effect of localized rugged topography on moisture sources that fed into the Aktoprak basin may be limited and go undetected in stable isotope studies.

6. Conclusions

All grey, carbonate-rich lacustrine sedimentary rocks of the Kurtulmuş Tepe Member section (~300 m) of the Aktoprak basin were remagnetized after tilting, whereas the pink rocks within the sequence carry a primary, pretilting magnetization.

The constructed magnetic polarity pattern, based solely on the pink, primary ChRM-carrying rocks in combination with biostratigraphic age controls, allows for the assignment of the section to the Late Oligocene (Chattian). The calculated sedimentation rate for our preferred correlation is 127 m/Ma, which suggests that the section was deposited over an interval of ~2.4 Ma.

The grey rocks are more carbonate rich than the pink rocks, suggesting that the extent of remagnetization was controlled in part by the material properties of the different rock types in the section.

The pink rocks that carry a primary ChRM are rich in clay minerals and may therefore have a lower porosity and permeability than the grey rocks. During burial and tectonic activity, the grey layers may have served as preferential pathways for fluid circulation, leading to the removal and neo-formation of magnetic grains. Removal of magnetic grains resulted in a significant drop in susceptibility and NRM intensity relative to the pink rocks, whereas the remagnetized directions are a CRM that is carried by the neo-formed magnetite minerals.

Carbon and oxygen isotopic results from the Kurtulmuş Tepe section show evidence for open freshwater lake conditions. The mean $\delta^{13}C_{V\text{-}PDB}$ and $\delta^{18}O_{V\text{-}SMOW}$ values are relatively constant throughout the section ($\delta^{13}C_{V\text{-}PDB} = -4.9 \pm 1.1‰$ and $\delta^{18}O_{V\text{-}SMOW} = 24.6 \pm 2.0‰$, N = 162), but the standard deviation of these values changes throughout the stratigraphy. The isotopic results also show short-lived evaporitic intervals—evidenced by increased $\delta^{18}O$ values—that are immediately followed by a shift toward open freshwater lake conditions.

The results from a ~50 m long section that was sampled for stable isotope analysis within the Kızılöz Member of the Aktoprak basin are very similar (mean $\delta^{13}C_{V\text{-}PDB} = -4.4 \pm 0.5‰$ and mean $\delta^{18}O_{V\text{-}SMOW} = 24.0 \pm 0.9‰$, N = 15) to the results of the Kurtulmuş Tepe section. If the isotopic values from the unexposed interval between the two sections are similar to the rocks studied here, then lake conditions remained very stable for an extended period of time.

$\delta^{18}O$ and $\delta^{13}C$ from the Kurtulmuş Tepe and Kızılöz sections concur with global and regional climate data that suggest that the Late Oligocene climate over Central Anatolia was subtropical.

A comparison between our isotopic results and the results from other Upper Oligocene to Middle Miocene Anatolian sections in lacustrine rocks by *Lüdecke et al.* [2013] shows that the Kurtulmuş Tepe and Kızılöz sections are very similar to those of the Chattian Mut basin and an Ecemiş corridor section. The similarity between the data sets is an additional suggestion that the Kurtulmuş Tepe section is indeed of Chattian age.

Our results for the Aktoprak basin indicate that no rain shadow or significant orographic barrier was present in Central Anatolia at the end of the Oligocene.

Acknowledgments

This research was funded by NSF grant EAR-1109762, "Continental Dynamics: Central Anatolian Tectonics (CD-CAT)" to Donna L. Whitney and by support of the Institute for Rock Magnetism by the NSF/EAR Instruments and Facilities program. Maud J.M. Meijers was supported by the College of Science and Engineering and Department of Earth Sciences at the University of Minnesota. Becky E. Strauss received support from the University of Minnesota Doctoral Dissertation Fellowship. Parts of this work were carried out in the Characterization Facility, University of Minnesota, which receives partial support from NSF through the MRSEC program. Andreas Mulch acknowledges support through the LOEWE initiative of Hesse's Ministry of Higher Education, Research, and the Arts. Satellite imagery is copyright DigitalGlobe, Inc., provided through the Polar Geospatial Center (University of Minnesota—Twin Cities) and processed by Côme Lefebvre. The authors would like to thank Katherine Hayes for providing the handheld XRF device and Jennifer H. Strehlau for magnetic extraction. Noah Keller, Pınar Ertepınar; Ullrich Treffert and Jens Fiebig are thanked for field and laboratory assistance. Discussions with Mike Jackson and Mark Bourne at the Institute for Rock Magnetism are much appreciated. We thank Ellen Platzman and an anonymous reviewer for their helpful comments. The data published in this study are listed in the supporting information tables.

References

Akgün, F., E. Akay, and B. Erdoğan (2002), Tertiary terrestrial to shallow marine deposition in Central Anatolia: A palynological approach, *Turk. J. Earth*, *11*, 127–160.

Akgün, F., M. S. Kayseri, and M. S. Akkiraz (2007), Palaeoclimatic evolution and vegetational changes during the Late Oligocene–Miocene period in Western and Central Anatolia (Turkey), *Palaeogeogr. Palaeoclimatol. Palaeoecol.*, *253*, 56–90, doi:10.1016/j.palaeo.2007.03.034.

Akkiraz, M. S., F. Akgün, T. Utescher, A. A. Bruch, and V. Mosbrugger (2011), Precipitation gradients during the Miocene in Western and Central Turkey as quantified from pollen data, *Palaeogeogr. Palaeoclimatol. Palaeoecol.*, *304*, 276–290, doi:10.1016/j.palaeo.2010.05.002.

Alan, I., B. Bakırhan, and H. Elibol (2011a), *Geological Map of Karaman—N32 Quadrangle*, Gen. Dir. of Miner. Res. and Explor. (MTA), Ankara.

Alan, I., Ş. Şahin, and B. Bakırhan (2011b), *Geological Map of Adana—N33 Quadrangle*, Gen. Dir. of Miner. Res. and Explor. (MTA), Ankara.

Atabey, E., M. C. Göncüoglu, and N. Turhan (1990), *Geological Map of Kazan—J19 Quadrangle (M33)*, Gen. Dir. of Miner. Res. and Explor. (MTA), Ankara.

Blumenthal, M. M. (1956), Yüksek Bolkardağın Kuzey Kenar Bölgelerin ve Bat Uzantların Jeolojisi, MTA yayılar, Series D, No. 7.

Blumstein, A. M., R. D. Elmore, M. H. Engel, C. Elliot, and A. Basu (2004), Paleomagnetic dating of burial diagenesis in Mississippian carbonates, Utah, *J. Geophys. Res.*, *109*, B04101, doi:10.1029/2003JB002698.

Butler, R. F. (1992), *Paleomagnetism: Magnetic Domains to Geologic Terranes*, 319 pp., Blackwell Sci., Boston.

Channell, J. E. T., D. A. Hodell, B. S. Singer, and C. Xuan (2010), Reconciling astrochronological and $^{40}Ar/^{39}Ar$ ages for the Matuyama-Brunhesboundary and late Matuyama Chron, *Geochem. Geophys. Geosyst.*, *11*, Q0AA12, doi:10.1029/2010GC003203.

Clark, M., and A. H. F. Robertson (2005), Uppermost Cretaceous–Lower Tertiary Ulukışla Basin, south-central Turkey: Sedimentary evolution of part of a unified basin complex within an evolving Neotethyan suture zone, *Sediment. Geol.*, *173*, 15–51, doi:10.1016/j.sedgeo.2003.12.010.

Clark, M. S., and A. H. F. Robertson (2002), The role of the Early Tertiary Ulukışla Basin, southern Turkey in suturing of the Mesozoic Tethys ocean, *J. Geol. Soc. London*, *159*, 673–690, doi:10.1144/0016-764902-015.

Creer, K. M., E. Irving, and A. E. M. Nairn (1959), Paleomagnetism of the Great Whin Sill, *Geophys. J. R. Astron. Soc.*, *2*, 306–323.

Demirtaşlı, E., N. Turhan, A. Z. Bilgin, and M. Selim (1984), Geology of the Bolkar Mountains, in Proceedings of the International Symposium on the Geology of the Taurus Belt, edited by O. Tekeli and M. C. Göncuoğlu, pp. 125–141, General Directorate of the Mineral Research & Exploration (MTA), Ankara.

Dewey, J. F., and A. M. C. Şengör (1979), Aegean and surrounding regions: Complex multiplate and continuum tectonics in a convergent zone, *Geol. Soc. Am. Bull.*, *90*, 84–92.

Fabian, K., V. P. Shcherbakov, and S. A. McEnroe (2013), Measuring the Curie temperature, *Geochem. Geophys. Geosyst.*, *14*, 947–961, doi:10.1029/2012GC004440.

Fisher, D. A. (1953), Dispersion on a sphere, *Proc. R. Soc. London, Ser. A*, *217*, 295–305.

Fortelius, M. (2013), New and Old Worlds (NOW) Database of Fossil Mammals, Univ. of Helsinki, NOW. [Available at http://www.helsinki.fi/science/now/.]

Galindo-Gonzalez, C., J. M. Feinberg, T. Kasama, L. C. Gontard, M. Posfai, I. Kosa, J. D. G. Duran, J. E. Gil, R. J. Harrison, and R. E. Dunin-Borkowski (2009), Magnetic and microscopic characterization of magnetite nanoparticles adhered to clay surfaces, *Am. Mineral.*, *94*(8-9), 1120–1129, doi:10.2138/am.2009.3167

Gierlowski-Kordesch, E. H. (2010), Lacustrine carbonates, in *Carbonates in Continental Settings: Facies, Environments and Progresses, Dev. Sedimentol.*, vol. 61, edited by A. M. Alonso-Zarza and L. H. Tanner, pp. 1–101, Elsevier, Amsterdam, doi:10.1016/S0070-4571(09)06101-9.

Göz, E., S. Kadir, A. Gürel, and M. Eren (2014), Geology, mineralogy, geochemistry, and depositional environment of a Late Miocene/Pliocene fluviolacustrine succession, Cappadocian Volcanic Province, central Anatolia, Turkey, Turk. *J. Earth Sci.*, *23*, 386–411, doi:10.3906/yer-1307-17.

Gülyüz, E., N. Kaymakci, M. J. M. Meijers, D. J. J. van Hinsbergen, C. Lefebvre, R. Vissers, B. Hendriks, and A. A. Peynircioglu (2013), Late Eocene evolution of the Çiçekdağı Basin (central Turkey): Syn-sedimentary compression during microcontinent–continent collision in central Anatolia, *Tectonophysics*, *602*, 286–299, doi:10.1016/j.tecto.2012.07.003.

Hayes, K. (2013), Parameters in the use of pXRF for archaeological site prospection: A case study at the Reaume Fort Site, Central Minnesota, *J. Archaeol. Sci.*, *40*, 3193–3211, doi:10.1016/j.jas.2013.04.008.

Hilgen, F. J., L. J. Lourens, J. A. Van Dam, A. G. Beu, A. F. Boyes, R. A. Cooper, W. Krijgsman, J. G. Ogg, W. E. Piller, and D. S. Wilson, (2012), Chapter 29—The Neogene Period, in *The Geologic Time Scale*, edited by F. M. Gradstein, et al., pp. 923–978, Elsevier, Boston, doi: 10.1016/B978-0-444-59425-9.00029-9.

Horita, J., and D. J. Wesolowski (1994), Liquid-vapor fractionation of oxygen and hydrogen isotopes of water from the freezing to the critical temperature, *Geochim. Cosmochim. Acta*, *58*, 3425–3437, doi:10.1016/0016-7037(94)90096-5.

Jackson, M., and N. L. Swanson-Hysell (2012), Rock magnetism of remagnetized carbonate rocks: Another look, in *Remagnetization and Chemical Alteration of Sedimentary Rocks*, edited by R. D. Elmore et al., *Geol. Soc. London Spec. Publ. 371*, pp. 229–251. doi:10.1144/SP371.3.

Jaffey, N., and A. Robertson (2005), Non-marine sedimentation associated with Oligocene-Recent exhumation and uplift of the Central Taurus Mountains, S Turkey, *Sediment. Geol.*, *173*, 53–89, doi:10.1016/j.sedgeo.2003.11.025.

Katz, B., R. D. Elmore, M. Cogioni, and S. Ferry (1998),Widespread chemical remagnetization: Orogenic fluids or burial diagenesis of clays?, *Geology*, *26*, 603–606.

Katz, B., R. D. Elmore, M. Cogioni, M. H. Engel, and S. Ferry (2000), Associations between burial diagenesis of smectite, chemical remagnetization, and magnetite authigenesis in the Vocontian trough, SE France, *J. Geophys. Res.*, *105*, 851–868.

Kaymakçı, N., Y. Özçelik, S. H. White, and P. M. Van Dijk (2009), Tectono-stratigraphy of the Çankiri Basin: Late Cretaceous to Early Miocene evolution of the Neotethyan Suture Zone in Turkey, in *Geodynamics of Collision and Collapse at the Africa-Arabia-Eurasia Subduction Zone*, vol. 311, edited by D. J. J. Van Hinsbergen, M. A. Edwards, and R. Govers, *311*, 67–106, Geol. Soc. of London, London, U. K, doi: 10.1144/SP311.3.

Kayseri-Özer, M. S. (2013), Spatial distribution of climatic conditions from the Middle Eocene to Late Miocene based on palynoflora in Central, Eastern and Western Anatolia, *Geodin. Acta*, *26*(1-2), 122–157, doi:10.1080/09853111.2013.877237.

Kelts, K., and M. Talbot (1990), Lacustrine carbonates as geochemical archives of environmental change and biotic/abiotic interactions, in *Large Lakes—Ecological Structures and Function*, edited by M. Tilzer and C. Serruya, pp. 288–315, Springer, Berlin, doi:10.1007/978-3-642-84077-7_15.

Kent, D. V. (1985), Thermoviscous remagnetization in some Appalachian limestones, *Geophys. Res. Lett.*, *12*, 805–808.

Kim, S. T., and J. R. O'Neil (1997), Equilibrium and nonequilibrium oxygen isotopic effects in synthetic carbonates, *Geochim. Cosmochim. Acta*, *61*, 3461–3475, doi:10.1016/S0016-7037(97)00169-5.

Kirschvink, J. L. (1980), The least-square line and plane and the analysis of paleomagnetic data, *Geophys. J. R. Astron. Soc.*, *62*, 699–718.

Koç, A., N. Kaymakcı, D. J. J. van Hinsbergen, K. F. Kuiper, and R. L. M. Vissers (2012), Tectono-sedimentary evolution and geochronology of the middle Miocene Altınapa basin, and implications for the late Cenozoic uplift history of the Taurides, southern Turkey, *Tectonophysics*, *532-535*, 134–155, doi:10.1016/j.tecto.2012.01.028.

Krijgsman, W., C. E. Duermeijer, C. G. Langreis, H. de Bruijn, G. Saraç, and P. A. M. Andriessen (1996), Magnetic polarity stratigraphy of late Oligocene to middle Miocene mammal-bearing continental deposits in Central Anatolia (Turkey), *Newsl. Stratigr.*, *34*, 13–29.

Lechler, A. R., and N. A. Niemi (2011), Controls on the spatial variability of modern meteoric δ^{18}O: Empirical constraints from the western U.S. and East Asia and implications for stable isotope studies, *Am. J. Sci.*, *311*(8), 664–700, doi:10.2475/08.2011.02.

Leng, M. J., and J. D. Marshall (2004), Palaeoclimate interpretation of stable isotope data from lake sediment archives, *Quat. Sci. Rev.*, *23*(7–8), 811–831, doi:10.1016/j.quascirev.2003.06.012.

Le Pennec, J.-L., A. Temel, J.-L. Froger, S. Sen, A. Gourgaud, and J.-L. Bourdier (2005), Stratigraphy and age of the Cappadocia ignimbrites, Turkey: Reconciling field constraints with paleontologic, radiochronologic, geochemical and paleomagnetic data, *J. Volcanol. Geotherm. Res.*, *141*(1–2), 45–64, doi:10.1016/j.jvolgeores.2004.09.004.

Li, H. C., and T. L. Ku (1997), δ^{13}C-δ^{18}O covariance as a paleohydrological indicator for closed-basin lakes, *Palaeogeogr. Palaeoclimatol. Palaeoecol.*, *133*, 69–80, doi:10.1016/S0031-0182(96)00153-8.

Lowrie, W. (1990), Identification of ferromagnetic minerals in a rock by coercitivity and unblocking temperature properties, *Geophys. Res. Lett.*, *17*, 159–162, doi:10.1029/GL017i002p00159.

Lüdecke, T., T. Mikes, B. Rojay, M. Cosca, and A. Mulch (2013), Stable isotope reconstruction of Oligo-Miocene paleoenvironment and paleohydrology of Central Anatolian lake basins (Turkey), *Turk. J. Earth Sci.*, *22*(5), 793–819, doi:10.3906/yer-1207-11.

Lüttig, G., and P. Steffens (1975), Paleogeographic Atlas of Turkey from the Oligocene to the Pleistocene, 7 maps, 64 p., Bundesanst. für Geowissenschaften und Rohstoffe, Hannover.

Machel, H. G., and P. A. Cavell (1999), Low-flux, tectonically-induced squeegee fluid flow ("hot flash") into the Rocky Mountain Foreland Basin, *Bull. Can. Pet. Geol.*, *47*, 510–533.

Mazzini, I., N. Hudáčková, P. Joniak, M. Kováčová, T. Mikes, A. Mulch, F. B. Rojay, S. Lucifora, D. Esu, and I. Soulié-Märsche (2013), Palaeoenvironmental and chronological constraints on the Tuğlu Formation (Çankırı Basin, Central Anatolia, Turkey), *Turk. J. Earth Sci.*, *22*(5), 747–777, doi:10.3906/yer-1207-10.

McCabe, C., and R. D. Elmore (1989), The occurence of Late Paleozoic remagnetization in the sedimentary rocks of North America, *Rev. Geophys.*, *27*, 471–494.

McFadden, P. L., and L. W. McElhinny (1988), The combined analysis of remagnetization circles and direct observations in palaeomagnetism, *Earth Planet. Sci. Lett.*, *87*, 161–172.

McFadden, P. L., and M. W. McElhinny (1990), Classification of the reversal test in palaeomagnetism, *Geophys. J. Int.*, *103*, 725–729.

McKenzie, J. A. (1985), Carbon isotopes and productivity in the lacustrine and marine environment, in *Chemical Processes in Lakes*, edited by W. Stumm, pp. 99–118, John Wiley, N. Y.

Meijers, M. J. M., N. Kaymakci, D. J. J. Van Hinsbergen, C. G. Langereis, R. A. Stephenson, and J.-C. Hippolyte (2010), Late Cretaceous to Paleocene oroclinal bending in the central Pontides (Turkey), *Tectonics*, *29*, TC4016, doi:10.1029/2009TC002620.

Nazik, A., and N. Gökçen (1992), Ostracoda genus Zonocypris and its species in Kurtulmuş Formation of Ulukışla Basin (Turkey), *Rev. Esp. Micropaleontol.*, *24*, 63–69.
Oktay, F. Y. (1982), Stratigraphy and geological evolution of Ulukişla and its surroundings, *Geol. Bull. Turk.*, *25*(1), 15–23.
Özdemir, Ö., and D. J. Dunlop (1996), Thermoremanence and Néel temperature of goethite, *Geophys. Res. Lett.*, *23*, 921–924, doi:10.1029/96GL00904.
Poage, M. A., and C. P. Chamberlain (2001), Empirical relationships between elevation and the stable isotope composition of precipitation and surface waters: Considerations for studies of paleoelevation change, *Am. J. Sci.*, *301*(1), 1–15, doi:10.2475/ajs.301.1.1.
Riveline, J., N. Gökcen, and A. Nazik (1990), Étude de la charoflore de la Kurtulmuş Tepe formation, bassin d'Ulukışla (Turquie), *Rev. Micropaléontol.*, *33*(1), 40–53.
Romanek, C. S., E. L. Grossmann, and J. W. Morse (1992), Carbon isotopic fractionation in synthetic aragonite and calcite: Effects of temperature and precipitation rate, *Geochim. Cosmochim. Acta*, *56*, 419–430, doi:10.1016/0016-7037(92)90142-6.
Schelske, C. L., and D. A. Hodell (1991), Recent changes in productivity and climate of Lake Ontario detected by isotopic analysis of sediments, *Limnol. Oceanogr.*, *36*, 961–975, doi:10.4319/lo.1991.36.5.0961.
Schemmel, F., T. Mikes, B. Rojay, and A. Mulch (2013), The impact of topography on isotopes in precipitation across the Central Anatolian Plateau (Turkey), *Am. J. Sci.*, *313*, 61–80, doi:10.2475/02.2013.01.
Schildgen, T. F., D. Cosentino, B. Bookhagen, S. Niedermann, C. Yıldırım, H. Echtler, H. Wittmann, and S. M. R. trecker (2012a), Multi-phased uplift of the southern margin of the Central Anatolian Plateau, Turkey: A record of tectonic and upper mantle processes, *Earth Planet. Sci. Lett.*, *317–318*, 85–95, doi:10.1016/j.epsl.2011.12.003.
Schildgen, T. F., D. Cosentino, A. Caruso, R. Buchwaldt, C. Yıldırım, S. A. Bowring, B. Rojay, H. Echtler, and M. R. Strecker (2012b), Surface expression of eastern Mediterranean slab dynamics: Neogene topographic and structural evolution of the southwest margin of the Central Anatolian Plateau, Turkey, *Tectonics*, *31*, TC2005, doi:10.1029/2011TC003021.
Schildgen, T. F., C. Yıldırım, D. Cosentino, and M. Strecker (2014), Linking slab break-off, Hellenic trench retreat, and uplift of the Central and Eastern Anatolian plateaus, *Earth Sci. Rev.*, *128*, 147–168, doi:10.1016/j.earscirev.2013.11.006.
Şengör, A. M. C., and Y. Yılmaz (1981), Tethyan evolution of Turkey: A plate tectonic approach, *Tectonophysics*, *75*(3–4), 181–241.
Şengör, A. M. C., N. Görür, and F. Saroğlu (1985), Strike-slip faulting and basin related formation in zones of tectonic escape: Turkey as a case study, in *Strike-Slip Deformation, Basin Formation, and Sedimentation*, edited by K. T. Biddle and N. Christie-Blick, *Soc. Econ. Paleontol. Mineral. Spec. Publ.*, *37*, 227–440.
Spötl, C., and T. W. Vennemann (2003), Continuous-flow isotope ratio mass spectroscopic analysis of carbon minerals, *Rapid Commun. Mass Spectrom.*, *17*, 1004–1006, doi:10.1002/rcm.1010.
Strehlau, J. H., L. A. Hegner, B. E. Strauss, J. M. Feinberg, and R. L. Penn (2014), Simple and efficient separation of magnetic minerals from speleothems and other carbonates, *J. Sediment. Res.*, *84*, 1096–1106.
Talbot, M. R. (1990), A review of the palaeohydrological interpretation of carbon and oxygen isotope ratios in primary lacustrine carbonates, *Chem. Geol.*, *80*, 261–279.
Talbot, M. R. and K. Kelts (1990), Paleolimnological signatures from carbon and oxygen isotopic ratios in carbonates from organic carbon-rich lacustrine sediments, in *Lacustrine Basin Exploration: Case Studies and Modern Analogs*, edited by B. J. Katz, *AAPG Mem.*, *50*, 88–112.
Tauxe, L., and D. V. Kent (2004), A simplified statistical model for the geomagnetic field and the detection of shallow bias in paleomagnetic inclinations: Was the ancient magnetic field dipolar?, in *Timescales of the Paleomagnetic Field 145, AGU Geophys. Monogr.*, edited by J. E. T. Channell et al., pp. 101–115, AGU, Washington, D. C.
Tauxe, L., K. P. Kodama, and D. V. Kent (2008), Testing corrections for paleomagnetic inclination error in sedimentary rocks: A comparative approach, *Phys. Earth Planet. Inter.*, *169*, 152–165.
Torsvik, T. H., et al. (2012), Phanerozoic polar wander, palaeogeography and dynamics, *Earth Sci. Rev.*, *114*, 325–368.
Tüysüz, O., A. A. Dellaloglu, and N. Tezioglu (1995), A magmatic belt within the Neo-Tethyan suture zone and its role in the tectonic evolution of northern Turkey, *Tectonophysics*, *243*, 173–191.
Ulu, Ü. (2009), Geological map of Karaman—M32 Quadrangle, Gen. Dir. of Miner. Res. and Explor. (MTA), Ankara.
Vandenberghe, N., F. J. Hilgen, R. P. Speijer, J. G. Ogg, F. M. Gradstein, O. Hammer, C. J. Hollis, and J. J. Hooker (2012), Chapter 28—The Paleogene Period, in *The Geologic Time Scale*, edited by F. M. Gradstein et al., pp. 855–921, Elsevier, Boston, doi:10.1016/B978-0-444-59425-9.00028-7.
Van Velzen, A. J., and J. D. A. Zijderveld (1995), Effects of weathering on single domain magnetite in early Pliocene marls, *Geophys. J. Int.*, *121*, 267–278.
Watson, G. (1983), Large sample theory of the Langevin distributions, *J. Stat. Plann. Inference*, *8*, 245–256.
Yıldırım, C., T. F. Schildgen, H. Echtler, D. Melnick, and M. R. Strecker (2011), Late Neogene orogenic uplift in the Central Pontides associated with the North Anatolian Fault—Implications for the northern margin of the Central Anatolian Plateau, Turkey, *Tectonics*, *30*, TC5005, doi:10.1029/2010TC002756.
Zachos, J., M. Pagani, L. Sloan, E. Thomas, and K. Billups (2001), Trends, rhythms, and aberrations in Global Climate 65 Ma to Present, *Science*, *292*, 686–693, doi:10.1126/science.1059412.
Zijderveld, J. D. A. (1967), A.C. demagnetization of rocks: Analysis of results, in *Methods in Palaeomagnetism*, edited by D. W. Collinson, K. M. Creer, and S. K. Runcorn, pp. 254–286, Elsevier, Amsterdam.